6-27-2016 12:00 AM

Establishing an In Vivo Model for Intratumoral Modulation Therapy for Glioblastoma Multiforme

Mitchell D. Cooper, *The University of Western Ontario*

Supervisor: Dr. Susanne Schmid, *The University of Western Ontario*

A thesis submitted in partial fulfillment of the requirements for the Master of Science degree in Anatomy and Cell Biology

Abstract

Glioblastoma multiforme (GBM) is the most common primary central nervous system tumor in adults, with an annual incidence of 3.0 per 100,000 of the population. Standard of care is a surgical resection of the tumor followed by adjuvant chemoradiation, but this treatment only offers patients a median lifespan of 12-18 months.

We propose an implanted device to deliver therapeutic high frequency electrical stimulation within the tumor-affected area of the brain, in a novel approach we refer to as Intratumoral Modulation Therapy (IMT). Our study aims to establish the effectiveness of this treatment in the F98 Fischer rat glioma model, a preclinical *in vivo* model of GBM.

Our data suggests that IMT attenuates tumor growth *in vivo*, which may result in better outcomes for patients with GBM or other tumors of the central nervous system. This may directly translate into a desperately needed novel multi-modal paradigm for GBM treatment.

Key Words: Glioblastoma, Electrotherapy, F98 glioma, Fischer rat, Intratumoral Modulation Therapy, Thionin staining, Cleaved caspase-3, Stereological analysis, Bioluminescence imaging, Magnetic resonance imaging

Acknowledgments

I would first like to thank my supervisors, Dr. Susanne Schmid and Dr. Matthew Hebb, for their mentorship and support. I deeply appreciate the effort spent nurturing my scientific skills and always being available to provide expertise or advice. I would also like to thank my supervisory committee, Dr. Alison Alan and Dr. Brian Allman, for their feedback and insight.

To all members of the Schmid and Hebb lab I give a huge thank you for helping make my Masters a great experience. I would like to give special thanks to Dr. Hu Xu, and Dr. Cleusa de Oliveira for their excellent training, support, and dependability, and to Dr. Andrea di Sebastiano for her expertise and assistance with experiments. I would like to thank Katie Parkins, Amanda Hamilton, and Dr. John Ronald for their equipment and assistance in bioluminescence imaging. Further, I would like to thank Miranda Bellyou, Dr. Robert Bartha, and Dr. Tim Scholl for their equipment and expertise in magnetic resonance imaging. I would also like to thank Amalka De Silva, Jason Gopaul, Andy Louttit, Erin Azzopardi, and Simon Benoit for their friendship, and assistance.

Lastly, I would like to thank my family for their love and constant support. I am extremely lucky and grateful to have them on my team.

Table of Contents

List of Tables

List of Figures

List of Abbreviations

Abbreviations	Term
AEF	Alternating electric field
BLI	Bioluminescence imaging
CNS	Central nervous system
DBS	Deep Brain Stimulation
EGFR	Epidermal growth factor receptor
FSE	Fast spin echo
FBS	Fetal bovine serum
FACS	Fluorescence activated cell sorting
GBM	Glioblastoma multiforme
IMT	Intratumoral modulation therapy
LOH	Loss of heterozygosity
MRI	Magnetic resonance imaging
MDM2	Mouse double minute 2
MGMT	Methylguanine methyltransferase
NF1	Neurofibromin-1
PBS	Phosphobuffer saline
PD	Parkinson disease
PDFα	Platelet derived factor α
PDFRα	Platelet derived factor receptor α
PFA	Paraformaldehyde
PTEN	Phosphotase and tensin homologue
Rb	Retinoblastoma

TMZ	Temozolomide
WHO	World Health Organization
7-AAD	7-aminoactinomycin D

PART 1: INTRODUCTION

Introduction

1.1 Glioblastoma multiforme

Primary brain tumors are responsible for approximately 2.3% of cancer related deaths in Europe and North America, and are one of the top ten causes of cancer related deaths(Canadian Cancer Society's Advisory Committee on Cancer Statistics, 2015). Gliomas are the most common form of primary brain tumors, and account for 80% of malignant central nervous system (CNS) tumors. Gliomas are defined as tumors with glial cell origins and include astrocytomas, oligodendrogliomas, and ependymomas(Agnihotri et al., 2013). Malignant gliomas are classified by the World Health Organization (WHO) into prognostic grades from I to IV based on histopathological features and clinical presentation(Louis et al., 2007). The most aggressive malignant astrocytoma, glioblastoma multiforme (WHO grade IV), is also the most common primary brain tumor and constitutes approximately 54% of all gliomas(Ostrom et al., 2013). In North America, the estimated incidence of glioblastoma multiforme (GBM) is 3.0 per 100,000 of the population(Louis et al., 2007). The prognosis for GBM is dismal, with a median lifespan of 12-15 months after time of diagnosis(Stupp et al., 2005).

In the past decade conventional therapies have failed to produce a meaningful improvement in lifespan due in part to the difficulty of developing drugs that can penetrate the blood brain barrier. Another challenge is the development of a treatment with tumor specificity despite the high intra and inter-tumor genetic and histological heterogeneity(Agnihotri et al., 2013; Holland, 2000).

1.1.1 Pathological Features

A GBM tumor mass typically develops in the subcortical white matter of the cerebral hemispheres, and is most often found in the fronto-temporal region. Occasionally a GBM will diffusely invade through the corpus callosum into the contralateral hemisphere, creating a bilateral, symmetrical lesion known as a butterfly glioma. Although GBM is exceptionally infiltrative, it rarely invades the subarachnoid space and thus normally does not metastasize through the cerebrospinal fluid(Louis et al., 2007).

GBM is exceptionally histologically heterogenous in nature and displays diffuse and rapid infiltrative proliferation of neighbouring brain structures. Grade I astrocytomas are benign and have relatively circumscribed borders, whereas grade II astrocytomas are characterized by moderate cellularity, little nuclear atypia, and are moderately proliferative and invasive. Further, grade III astrocytomas possess increased cellularity, nuclear atypia, and mitotic division. Similar to anaplastic astrocytomas (WHO grade III), GBM is characterized histologically by the presence of increased cellularity, nuclear atypia, and mitotic activity(Agnihotri et al., 2013). GBM is distinguished from lower grade astrocytomas by the presence of necrosis and substantial microvascular invasion. Moreover, GBM is markedly more aggressive than lower grade astrocytomas, displaying a higher rate of proliferation, invasiveness, and angiogenesis(Holland, 2000).

Depending on the origin of the tumor, GBM can be divided into primary or secondary subtypes. These subtypes differ in both their clinical presentation and molecular characteristics. Although both subtypes appear indistinguishable at a histological and morphological level, they have distinct and notable genetic differences(Agnihotri et al., 2013).

Primary GBM tumors arise *de novo*, meaning spontaneously, and account for 95% of all cases of GBM(Ohgaki et al., 2004). This subtype is characterized by gene amplification of epidermal growth factor receptor (EGFR); loss of heterozygosity (LOH) of chromosome 10q containing phosphatase and tensin homolog (PTEN); overexpression of mouse double minute 2 (MDM2), and deletion of p16(Furnari et al., 2007; Wen & Kesari, 2008).

Secondary GBM tumors account for 5% of GBM cases, are most often found in patients under the age of 45, and progress from lower grade astrocytomas into GBM. These tumors are characterized by mutations of TP53 and retinoblastoma (Rb); overexpression of platelet-derived growth factor A and platelet-derived growth factor receptor alpha (PDGFα/PDGFRα), and LOH of 19q(Furnari et al., 2007; Wen & Kesari, 2008). The prognosis for secondary glioblastomas tends to be marginally better than the primary subtype, although this may be because the average age of diagnosis in secondary GBM is younger(Holland, 2000).

Genomic analysis has revealed four major molecular subtypes for GBM, which have been classified as classical, mesenchymal, proneural, and neural. These subtypes are distinguished by differential gene expression of EGFR, Neurofibromin-1 (NF1), PDGFRα, and ERBB2 respectively. Interestingly, these subtypes have been proven to have varying responses to chemotherapy and radiation(Verma, 2009). The vast molecular heterogeneity between subtypes has made it exceptionally difficult to find widely expressed molecular targets for therapeutics. Further complicating the issue are genetic differences found within GBM subpopulations that have been shown to affect patient prognosis. The most common instance of this is the silencing of the DNA repair enzyme

O^6-methylguanine DNA methyltransferase (MGMT) through methylation of its promoter. After receiving radiation and the chemotherapeutic temolozolomide (TMZ), patients who have a methylated MGMT promoter live on average 9 months longer than patients without the promoter methylation(Agnihotri et al., 2013).

1.1.2 Epidemiological Features

GBM can develop at any age, but is most typically found in adults between the ages of 45-75 years old. A population-based study in Switzerland found the mean age of diagnosis is 61.3 years. Over 80% of patients diagnosed were over 50 years old, while only 1% of patients were under 20(Louis et al., 2007). GBM has a slightly higher incidence in males than females, with a male:female ratio of 1.26(Ostrom et al., 2013). A majority of gliomas appear to have no underlying carcinogenic cause. However, exposure to high-dose, ionizing radiation has been established to increase the risk of developing a glioma(Bondy et al., 2008; Verma, 2009). The occurrence of glioma in multiple members of one family is rare, but seen in approximately 5-10% of glioma cases(Fisher et al., 2007). Generally, this is observed with inherited tumor syndromes such as Turcot and Li-Fraumeni syndromes, neurofibromatosis type 1, and multiple enchondromatosis(Bondy et al., 2008; Verma, 2009).

1.1.3 Clinical Presentation and Treatment

The current standard therapy for newly diagnosed GBM is maximal surgical resection, followed by adjuvant chemotherapy and radiotherapy(Nabors et al., 2014). Despite aggressive resection, the tumor's invasiveness and diffuse borders make complete tumor resection impossible. In fact, approximately 90% of resected tumors will recur at the site of the resection(Berens & Giese, 1999).

Despite decades of research, the prognosis for GBM has remained bleak, and overall survival in patients has barely improved. Stupp et al.(2005), demonstrated that concomitant radiation and chemotherapeutic TMZ, followed by adjuvant TMZ, increased median overall survival from 12.1 to 14.6 months compared to radiation alone. Consequently, this has become the standard of care for newly diagnosed GBM patients following surgical resection(Nabors et al., 2014).

1.2 Animal Brain Tumor Models

Animal brain tumor models are necessary to progress our understanding of neuro-oncology, and to serve as preclinical tests for novel brain tumor therapies. Rat brain tumor models have been extensively studied since the 1970s and have been used successfully to determine the efficacy of brain tumor therapies(Barth & Kaur, 2009). In the 1970s it was reported that brain tumors could be consistently reproduced in adult rats by injecting n-Ethyl-Nitrosourea weekly. These tumors were then harvested, cloned, and reimplanted into other rats, providing reliable and reproducible models(Barth & Kaur, 1998).

Rat tumor models are considered to be most effective when assessing the efficacy of therapeutics, whereas mouse models are best suited for elucidating the importance of specific cancer related genes(Barth & Kaur, 2009). Mouse tumor models are easier to genetically manipulate, letting researchers generate tumors with specific genetic alterations and controlled environment influences(Reilly et al., 2008). Rats have a relative lack of genetic manipulability compared to mice, and so are less effective when studying specific genetic factors. However, rat models have larger brains for more precise

stereotactic injections, larger tumor sizes for easier *in vivo* localization and imaging, and more extensive characterization in the literature *in vitro* and *in vivo*(Barth & Kaur, 2009).

Currently, most preclinical brain tumor research uses implantation models. Implantation glioma models are much simpler to use and are relatively inexpensive to develop and maintain compared to other *in vivo* models like transgenic models (Lampson, 2001; Peterson, Snerioan, Ph, & Brown, 1994). Transgenic tumors are genetically diverse and highly variable, and are most well-suited to investigate specific genetic factors underlying tumor initiation and progression. Implantation models, where cultured cancer cell lines are implanted into an animal, are useful when evaluating the efficacy of a novel treatment(Kobayashi, Allen, Clendenon, & Ko, 1980; Lampson, 2001; Peterson et al., 1994).

1.2.1 Rat tumor model criteria

Although no rat brain tumor model will accurately encompass all features of a human GBM tumor, it must meet specific criteria to be considered an analogous model. No animal model perfectly replicates its human counterpart, but it should be as close as possible to reproduce the clinical scenario. For this reason, in a rat glioma model the tumor cells must be originally derived from glial cells, and should still be able to grow as cell lines *in vitro* as well as rapidly proliferate *in vivo*. To produce consistent and testable results, the tumor growth rates in the brain should be predictable and reliable. Further, these tumors must exhibit the classical pathological features of GBM, should not metastasize outside the brain, and should show a similar resistance to treatment as human GBM(Lampson, 2001; Mathieu et al., 2007; Peterson et al., 1994; Rama et al., 1986).

1.2.2 Rat models of GBM

A multitude of rat models have been used to study GBM, and they each confer particular advantages and disadvantages. Certain models have been particularly well-studied due to their ease of use, and similarity to human GBM. The C6 rat glioma model has been extensively used in experimental neuro-oncology to assess the efficacy of a wide range of conventional and experimental therapeutics(Doblas et al., 2008; Tanriover et al., 2008). C6 glioma cells have been molecularly characterized and show changes in gene expression similar to human glioblastomas(Guo et al., 2003; Heimberger, et al., 2005). However, a major drawback of the C6 glioma rat model is its high immunogenicity in all rat strains, due to its origin from outbred Wistar rats(Grobben et al., 2002). Wistar rats injected with C6 glioma cells either intracerebrally or subcutaneously demonstrate a profound immune response to the tumors(Parsa et al., 2000). The high immunogenicity of the C6 glioma model does not accurately reflect the low immune response found in human GBM, and thus may overestimate the efficacy of novel therapeutics. Accordingly, *in vivo* studies showing remarkable responses to therapy in the C6 glioma model have not translated into human patients(Grobben et al., 2002; Parsa et al., 2000; Tonn 2002). Despite this flaw, the C6 glioma model has remained an excellent model to study brain tumor biology and has been used to study numerous facets of brain tumor growth and proliferation(Li et al., 2013; Miyake, Benadiba, Ribeiro, De Oliveira Silva, & Colquhoun, 2014).

Similar to the C6 rat glioma model, the 9L rat gliosarcoma model has been widely used to study brain tumors. Unlike human GBM, the 9L gliosarcoma tumor has sharply delineated borders and does not demonstrate obvious invasion into the brain

parenchyma(Barth & Kaur 2009). The 9L glioma cells were originally derived from a Fischer rat brain tumor, and are implanted into syngeneic Fischer rat hosts to test therapeutics or investigate tumor cell biology(Barker, Hoshino, Gurcay, & Eliason, 1973; Saini, Roser, Samii, & Bellinzona, 2004). Although multiple studies have shown impressive therapeutic results using the 9L model, the cells have been confirmed to be immunogenic and appear to mediate a T-cell anti-tumor response(Denlinger et al. 1975; Morantz et al. 1979). Much like the C6 model, the activated immune system potentiates the effect of novel therapeutics and therefore does not accurately reflect the low immunogenicity of human glioblastomas(Mcgarrity & Chiang 1995). This has limited the use of the 9L model to investigating basic tumor biology(Schepkin et al., 2011).

The F98 glioma model consists of implanting glioma cells originally derived from a Fischer rat, back into syngeneic Fischer rat hosts. F98 tumors show extensive invasion into normal brain parenchyma, with groups of tumor cells extending out from the tumor mass and forming perivascular clusters(Barth & Kaur 2009). These tumors are histopathologically similar to human glioblastomas as they form necrotic cores, contain highly mitotic cells, and show non-glomeruloid neovascular proliferation(Mathieu et al., 2007). Like human glioblastomas, molecular characterization of F98 cells revealed overexpression of PDGFβ, and EGFR(Sibenaller et al., 2005).

This model is considered to be an excellent representation of human glioblastomas because it models both the low immunogenicity, as well as the high invasive pattern of growth found in humans. The low immunogenicity is critical for evaluating the efficacy of novel therapeutic agents, ensuring that most of the tumor cell death is caused by the treatment and not the immune system. Further, F98 gliomas in rats have been shown to

be unresponsive to systemic chemotherapy and photon-irradiation alone, replicating the refractory nature of human GBM(Barth & Kaur 2009; von Eckardstein et al. 2005).

The F98 glioma model has been widely used in conjunction with MRI to investigate *in vivo* tumor growth in a living rat(Blanchard, Mathieu, Patenaude, & Fortin, 2006). Moreover, the F98 cell line can be stably transfected with the luciferase gene to produce a bioluminescent cell line(Bryant, Chuah, Luff, Lavin, & Walker, 2008). These cells can be implanted into Fischer rat brains, and tumor size and progression can be non-invasively monitored by measuring photons emitted by the cells. Consequently, well-established multi-modal imaging enables a reliable estimation of therapeutic efficacy.

In order to compare treatment effect between animals, there is a need for consistent tumor take and growth in order to precisely measure therapeutic efficacy. To address this need, Mathieu et al (2005; 2007) established an implantation procedure for F98 cells in Fischer rats standardizing the number of F98 cells injected, and stereotactic injection coordinate. This standardized model of injection resulted in 100% tumor uptake, and demonstrated highly reproducible tumor growth. The reproducibility of the F98 model combined with its clinical and pathophysiological similarities to human GBM makes it an excellent preclinical model to test novel GBM therapeutics.

1.3 Electrotherapy

Electrotherapy is a common form of treatment used for certain movement disorders, such as Parkinson Disease (PD), and has been used successfully for decades to safely manage disease symptoms and improve clinical outcomes(Pereira, Green, Nandi, & Aziz, 2007). Recently, electrotherapy has also been explored as an alternative treatment modality for

neoplastic disease. Electrotherapeutics have been widely shown to exert anti-tumor effects on numerous types of cancer *in vitro* and *in vivo*, but the clinical use of electrotherapeutics remains uncommon in the treatment of cancer(Guo et al. 2014; Neal et al. 2014; Sersa et al. 2015; Tang et al. 2009). The mechanism by which these anti-cancer electrotherapies work differs based on the intensity and frequency of the electric pulses delivered. The effect of electrical stimulation delivered at different parameters to cells has been comprehensively studied in the literature(McCaig, Rajnicek, Song, & Zhao, 2005). At frequencies under 1kHz, electrical pulses depolarize the cell membrane of neurons and can induce action potentials(Repacholi & Greenebaum 1999). High intensity stimulation around a kV/cm and high frequency fields in the MHz to GHz range generate enough heat to destabilize cell membranes and lead to cell death(Markx, 2008). Intermediate frequencies of electric stimulation between 10 kHz and 1 Mhz are too rapid to stimulate neurons, and too low frequency to generate significant heat. Accordingly, stimulation in this range was long believed to be biologically inert(Giladi et al., 2015).

1.3.1 Previous electrotherapies to treat GBM

Electroporation is a form of electrotherapy which has been investigated as a potential treatment for GBM. Electroporation entails delivering short bursts of high voltage pulses to generate transient, reversible pores in the cell membrane(Gehl, 2003). These pores facilitate the uptake of chemotherapeutic agents, in a process termed electrochemotherapy, or lead to metabolic instability and cell death. Preclinical *in vitro* studies showed that four to eight electroporating pulses, ranging in intensity from 1000-1750V/cm, reduced GBM cell viability and increased chemosensitivity. Further, *in vivo* studies demonstrated that eight 400V pulse trains delivered into a rat glioma,

concurrently with the chemotherapeutic bleomycin, prolonged animal survival, and enhanced gene therapy(Horikoshi, Naganuma, Ohashi, Ueno, & Nukui, 2000; Orlowski, Belehradek, Paoletti, & Mir, 1988; Zimmermann, 1982). Despite electroporation's proven efficacy in preclinical models, the extremely high stimulation intensity needed affects neoplastic and non-neoplastic cells alike, therefore limiting its usage in a human GBM patient. The potential unintended damage to normal brain parenchyma presents unacceptable safety concerns when considering electroporation in a human GBM patient. Moreover, the lack of specificity is particularly restrictive if the tumor is diffuse or in eloquent regions of the brain(Pudenz, 1976).

1.3.2 Development of alternating electric fields

In 2004 Kirson et al., (2004) first investigated the anti-cancer potential of intermediate frequency electrical stimulation previously believed to be biologically inert. Human and animal cancer cell lines were stimulated at frequencies ranging from 100-500 kHz through insulated wires attached to the bottom of cell culture wells. The stimulation pulses were staggered between the two electrodes to generate alternating electric fields (AEFs), and significantly reduced cell viability across all cell lines tested(Kirson et al., 2004). Interestingly, different cell lines exhibited varying sensitivities to different frequencies. It was found that the optimal frequency to target glioma cells was 200 kHz. In both mouse subcutaneous tumors and rat gliomas, AEFs inhibited tumor growth and had an additive cytotoxic effect with certain chemotherapies(Kirson et al., 2007).

1.3.3 Cytotoxic mechanism of alternating electric fields

The mechanism behind AEFs tumor killing effect is still not completely clear, though evidence suggests it is at least partially caused by disruption of charged intracellular

molecules responsible for mitosis(Rehman et al. 2015). Mitotic cells contain a considerable amount of highly polar microtubules, which form the spindle apparatus necessary to undergo normal mitotic division(McIntosh et al. 2002). It is hypothesized that AEFs act on these electrically charged molecules by altering their orientation and location in the cell, thus disrupting the cellular machinery needed to replicate. Microphotography of cancer cells treated with AEFs show abnormalities suggestive of aberrant mitosis such as aneuploidy and membrane blebbing in anaphase(Giladi et al., 2015; Kirson et al., 2004). Further, AEFs have been shown to destabilize microtubule formation in dividing cells, thereby increasing the amount of depolymerized tubulin in AEF affected cells. This corresponded with a rise in caspase dependent apoptosis, ultimately leading to reduced cell viability. Moreover, cytotoxicity was dependent on cell doubling time, with faster dividing cells being more susceptible to treatment(Giladi et al., 2015). This reinforces the theory that the treatment targets cells undergoing mitosis exclusively, and would therefore leave post-mitotic cells like neurons unaffected.

1.3.4 Clinical studies of alternating electric fields

Due to the promising results in preclinical studies, a pilot study was created for 10 recurrent GBM patients to receive AEFs in monotherapy. The stimulation was delivered by four transducer pads attached to their shaved skull, at 1-2 V/cm and 200 kHz(Kirson et al., 2007). These parameters were used as they were previously shown to be the optimal frequency to treat gliomas in experimental preclinical trials(Kirson et al., 2004). The results seemed encouraging when compared with historical controls, with an increase in progress free survival, and overall survival (62.2 vs 29.3 weeks, Kirson et al., 2007). However, a follow-up Phase III randomized clinical trial showed a much less favourable

response. 237 patients were treated with AEF monotherapy, and 117 were assigned physician's choice chemotherapy(Stupp et al., 2012). There was no statistical difference in median overall survival (6.6 vs 6.0 months), progression free survival, radiological response rate or one year survival rate. Nevertheless, the external device delivering the AEFs is now FDA-approved.

Despite the negative results, adverse side effects caused by AEFs were reported to be significantly lower than in the chemotherapy group, and quality of life questionnaires favoured AEFs over the chemotherapy group(Stupp et al., 2012). Recently in a multisite randomized clinical trial, adult GBM patients were randomized to receive treatment of AEFs and TMZ (n=486) or TMZ alone (n=229). An interim analysis of the trial has shown promising results, with a significant improvement for the combined AEF/TMZ group compared to TMZ alone in progression free survival (7.1 vs 4.0 months), and overall survival (20.5 vs 15.6 months, Stupp et al. 2015). These results, though only preliminary, are promising as the life expectancy of patients with GBM has remained nearly unchanged in the past decade.

1.3.5 Limitations of the FDA-approved device delivering alternating electric fields

Despite these positive results, the largest limitation of the device is achieving patient compliance. Due to the externalized nature of the apparatus that delivers the AEFs, there is a heavy burden on the patient to ensure the treatment is being delivered effectively. Patients must strictly adhere to proper maintenance of management of the device to ensure the optimal therapeutic dosage is delivered. Furthermore, the obvious appearance of the device coupled with the need to constantly shave one's head may stigmatize the patient and further discourage proper use. Accordingly, patient compliance has been very

poor, with more than 20% of patients originally assigned to AEF monotherapy in the Phase III trial opting to discontinue treatment earlier than expected(Stupp et al., 2012).

1.4 Rationale

Preclinical and clinical data demonstrate significant potential for the use of electrotherapy as a new modality to treat GBM, yet existing therapeutics have drawbacks that limit their clinical applicability and efficacy. The effectiveness of AEFs may be compromised by the inability to precisely target fields to deliver maximum treatment intensity and avoid off-target injury. Further, the externalized nature of the device stigmatizes the patient, and present an unacceptable burden. Neuromodulation therapy is the delivery of targeted low intensity electrical stimulation to the brain through implanted electrodes, and has become the surgical standard of care, in the form of deep brain stimulation, for certain neurological diseases such as PD. The treatment procedure used in PD is known as deep brain stimulation (DBS) and typically entails implantation of a multi-contact lead into the subthalamic nucleus or globus pallidus. The lead is controlled by a pulse generator located subcutaneously in the chest, which delivers therapeutic low voltage stimulation with a frequency of approximately 100-300 Hz(The Deep-Brain Stimulation for Parkinson's Disease Study Group 2001). The mechanism by which DBS works is not well-understood, but its effects do not appear cytotoxic to normal brain tissue(Deniau, Degos, Bosch, & Maurice, 2010). Our lab has proposed to use an implantable device to deliver therapeutic electrical stimulation directly into the tumor-affected region of the brain. The stimulation delivered is analogous to the AEFs show to be efficient in treating GBM. This device may exploit the known electrosensitivity of GBM cells, while improving the limitations found in other electrotherapeutics. This approach confers many

benefits, such as a lack of stigma due to the concealed internalized nature of the device. Further, an implanted device permits a more focused, and sustained approach with low maintenance for a patient, and the capability to target infratentorial tumours. When used in the treatment of neoplastic disease we refer to this approach as intratumoral modulation therapy (IMT).

To date, the effect of IMT has been extensively evaluated by our lab *in vitro* and found to have a selective cytotoxic effect on human cancer cell lines, and primary human GBM cells, while not affecting neuronal cell viability (**Figure 1, Figure 2)**. This study aimed to develop an *in vitro* proof of principle model of IMT to investigate any potential anti-cancer effects of IMT. The IMT model was composed of a central stimulating electrode in the center of a 35mm well, and a reference strip electrode around the periphery of the well. This electrode configuration permits the therapeutic stimulation to travel in equal radial directions outward from the center of the dish, thus encompassing the entirety of the well with stimulation. In addition to its selective antitumor effect, IMT appears to potentiate the effect of TMZ and gene therapy *in vitro*, and kill cells in an apoptosis dependent manner(Xu et al., 2016). The promising effect of IMT alone, and in conjunction with existing and experimental therapies warrants further studies to develop the treatment. However, the effect of IMT in a glioma animal model has not yet been studied. Although the findings *in vitro* are encouraging, corroborating these results in an animal model would strengthen the evidence supporting IMT. Therefore, determining the efficacy and safety of IMT in a living animal is a crucial preclinical step before translation of this treatment paradigm into humans.

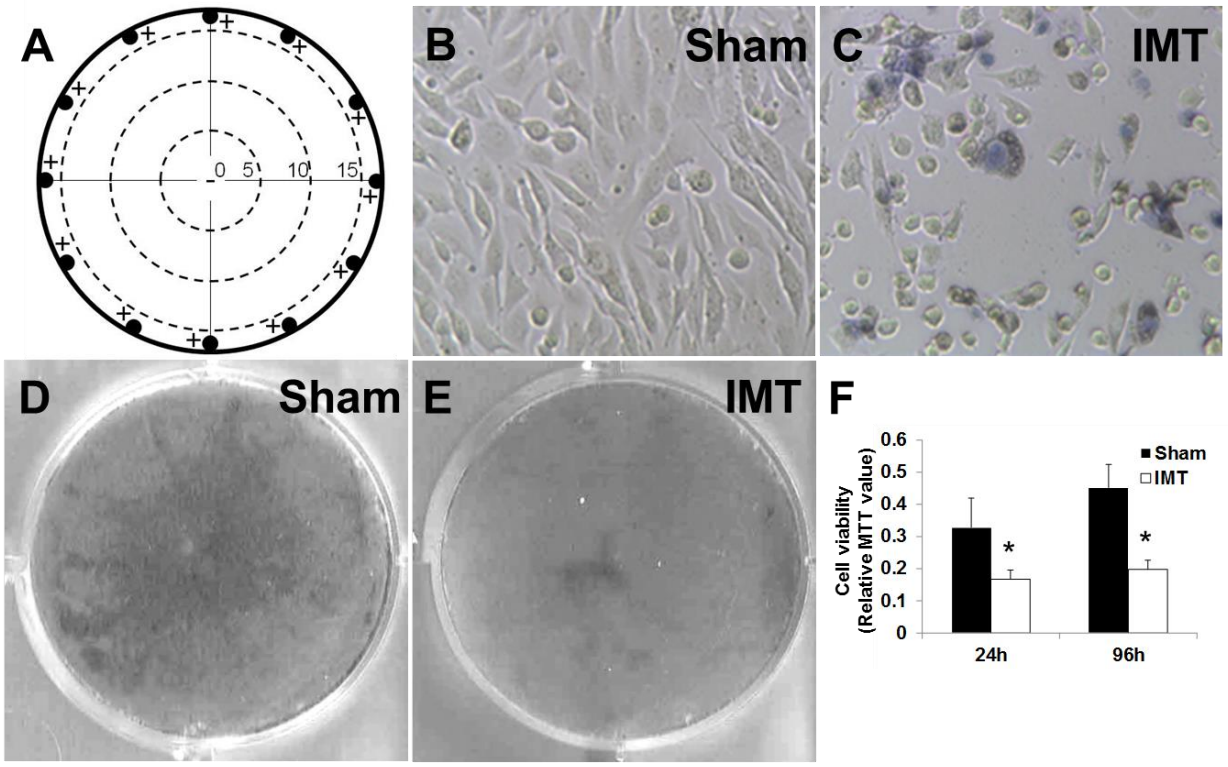

Figure 1. In Vitro model of IMT

A) Schematic representation of in vitro IMT. Wells fitted with a central stimulating electrode and peripheral reference electrodes delivered IMT to GBM cells. Primary GBM cultures 48 hours following B) sham treatment (electrode apparatus, but no stimulation) or C) IMT, labelled with trypan blue exclusion dye. Cells treated with IMT showed reduced cell density, and increased uptake of trypan blue dye. Cell viability was assessed using an MTT assay in both D) sham and E) IMT treated conditions. F) Mean cell viability was significantly reduced after both 24 and 96 hours of IMT (Adapted with permission from Xu et al., 2016).

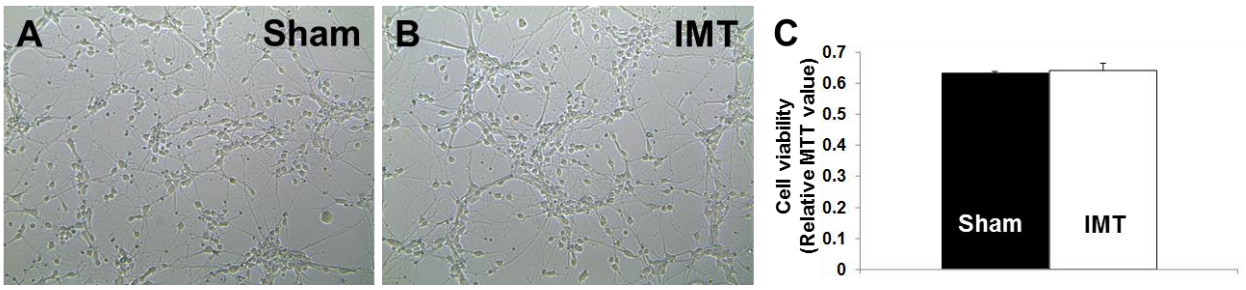

Figure 2. IMT has no significant cytotoxic effect in post-mitotic neurons

Brightfield microscopy pictures of embryonic rat neuronal cultures treated for 72 hrs with A) sham and B) IMT and exposed to trypan blue dye. No significant changes in cell viability or morphology were apparent after IMT compared to sham conditions. C) Relative cell viability was measured using the MTT assay. No significant difference was found between sham and IMT groups (Adapted with permission from Xu et al., 2016).

1.5 Hypothesis

We hypothesize that an *in vivo* model of IMT will have a therapeutic effect in the well-characterized F98 Fischer rat glioma model. IMT has an anti-cancer effect *in vitro* when delivered at the parameters 130 Hz, and 200 kHz. The parameters for 130 Hz stimulation is used in DBS and known to be generally safe, whereas the parameters for 200 kHz are supposedly biologically inert and outside the frequency to entrain neuronal activity, and therefore will not unwantedly activate neurons. We suggest that IMT delivered at 200 kHz will have a selective cytotoxic effect on glioma cells, while sparing post-mitotic neurons in our *in vivo* animal model.

1.6 Objectives

1. Establish a proof of principle model of IMT in the F98 Fischer glioma model, and demonstrate its safety and efficacy.
2. Through the use of various imaging modalities, establish non-invasive methods to evaluate the progression of tumor growth in the F98 Fischer glioma model.

PART 2: METHODS

Methods

2.1 F98 Cell Preparation

F98 rat glioma cells (ATCC, Manassas, VA, USA) were purchased and stored at -20˚C until use. The cells were grown in DMEM with 10% Fetal Bovine Serum (FBS), 1% non-essential amino acids and 1% penicillin/streptomycin (Life Technologies, Carlsbad, CA) at 37˚C in a humidified atmosphere of 5% CO_2. At approximately 80% confluence the cells were passaged using 0.25% trypsin-EDTA (Wisent, Saint-Jean-Baptiste, QC). On the day of surgery, cells in their exponential growth phase had their medium removed and were washed with PBS two times. The cells were then digested with trypsin-EDTA for approximately 5 minutes, before supplemented DMEM was re-added to inactivate trypsin activity. The resulting solution was transferred to a falcon tube and centrifuged at 1200 rotations per minute for five minutes. Another 10 mL of DMEM was added to the solution, and then the solution was pipetted up and down repeatedly. The total cell number was counted on a cell counter and then washed two more times with PBS. A proportionate amount of PBS was then added to make the cell concentration 20,000 cells per microliter. Cells in PBS were put on ice and were then immediately transferred to the surgery room for injection.

2.2 Animals and Surgical Procedures

All procedures followed the guidelines of Canadian Council on Animal Care and Western University Animal Care Committee. Approximately 3-6 month old Fischer rats (Charles River Canada) were housed in pairs and had food and water provided *ad libitum*. Rats were allowed to habituate to their new environment for at least one week prior to surgery.

Rats were anesthetized with 5% isoflurane (University Hospital Pharmacy, London, ON) and 2% oxygen, and were transferred to a stereotactic frame. Their heads were stabilized in the frame using ear bars and the mouth piece, and they were kept under anesthesia throughout the surgery by maintained delivery of 2% isoflurane and 1% oxygen through a mouth piece. Body temperature was maintained by an isothermic pad warmed to approximately 37˚C. The rats were then shaved at the top of their heads, and the shaved area was sterilized with soap, ethanol, and iodine. Rats were administered 0.1mL/100g meloxicam and 0.1mL/100g baytril subcutaneously, and a midline scalp incision was made in the sterilized area. Bregma was set with stereotaxic units AP: 0mm, ML: 0 mm, DV: 0 mm. Three jeweler screws were set into the skull to anchor the head cap. Bilateral burrholes were drilled in the skull and cannula/electrode constructs (custom built by PlasticsOne, Roanoke, VA) were implanted into the caudate putamen with the coordinates AP: 1mm, ML: +/-3mm, DV: 6mm.

The cannula electrode constructs had an electrode attached to the guide cannula to allow infusion of F98 cells through the cannula and subsequent delivery of IMT to the center of the tumor. A reference electrode attached to the construct was implanted subcutaneously under the nuchal tissue at the caudal end of the incision site. The cannula/electrode construct was then secured to the skull with dental cement. Over the course of five minutes, two 2µL deposits of DMEM containing 40,000 F98 glioma cells were bilaterally injected using Hamilton syringes (Hamilton Company, Reno, NV) connected to an injector inserted in the guide cannula via thin plastic tubing (PlasticsOne, Roanoke, VA). Injections were performed over a time period of 7 minutes using a micro-infusion pump (KDScientific, Holliston, MA) with two operators present. The injectors were kept in

place for two minutes after the injection was completed, to ensure minimal cell backflow. Following their removal, the injectors were replaced with sterile threaded dummy stylets (PlasticsOne, Roanoke, VA) screwed into the cannula electrode constructs. The incision was sutured and 3mL of warm sterile saline was administered subcutaneously.

After surgery, the animal was monitored in a recovery cage with a heating lamp until it awoke from anesthesia, and it was subsequently transferred into a housing cage with soft bedding. In order to assess the effect of IMT on normal brain parenchyma, in some control animals the entire surgery was performed as detailed above, except no F98 cells were injected in either brain hemisphere. In order to establish baseline tumor size at various time points after surgery, in some animals the entire surgery was performed as previously detailed, but no cannula/electrodes were implanted, and a unilateral 2 µL deposit of 40,000 F98 cells was injected by a Hamilton syringe directly into the target coordinates. The baseline tumor size at various time points was also non-invasively imaged using MRI and BLI **(Table 1)**.

2.3 Initiation of Intratumoral Modulation Therapy

Four days following surgery, one cannula/electrode construct was randomly chosen to receive stimulation, while the other side acted as a sham control. The dummy cap from the chosen cannula/electrode construct was removed, and replaced with a connector to the stimulation and reference electrode, tethered with a suspended commutator on the ceiling of the cage (PlasticsOne, Roanoke, VA) attached to a waveform generator (Rigol, China), permitting the animal free range of motion in its cage during treatment. Unilateral stimulation (sine wave, 200kHz, +/- 2V) was delivered to the stimulating electrode continuously for seven days. Animals receiving IMT did not show signs of distress or neurological symptoms while the treatment was being delivered **(Figure 3, Figure 4)**. Rigorous quality control safeguards were developed during the course of this thesis work to ensure stimulation was appropriately delivered over the time course of the experiment. The entire stimulating apparatus was assembled and attached to the waveform generator before implantation of the cannula electrode into the rat. The stimulating electrode was measured with an oscilloscope to ensure current could flow through the entire apparatus. After initiation of IMT, the waveform generator was directly measured with an oscilloscope every day to ensure current was still being driven through the apparatus. Finally, after termination of the experiment the cannula electrode was extracted from the animal and the entire apparatus was re-measured with an oscilloscope to ensure the electrode hadn’t been damaged during the course of the IMT.

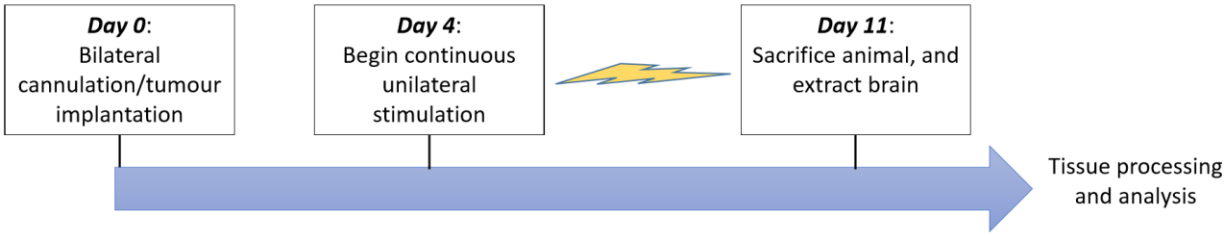

Figure 3. Surgical and therapeutic timeline for in vivo IMT.

At day 0, electrode cannula constructs were bilaterally implanted into the caudate putamen of Fischer rats, and 40,000 F98 cells were injected bilaterally through the cannula. Four days were given for tumor growth to occur and to let the rats recover before unilateral IMT stimulation began. After 7 days of continuous unilateral stimulation animals were sacrificed and brain tissue was harvested for analysis.

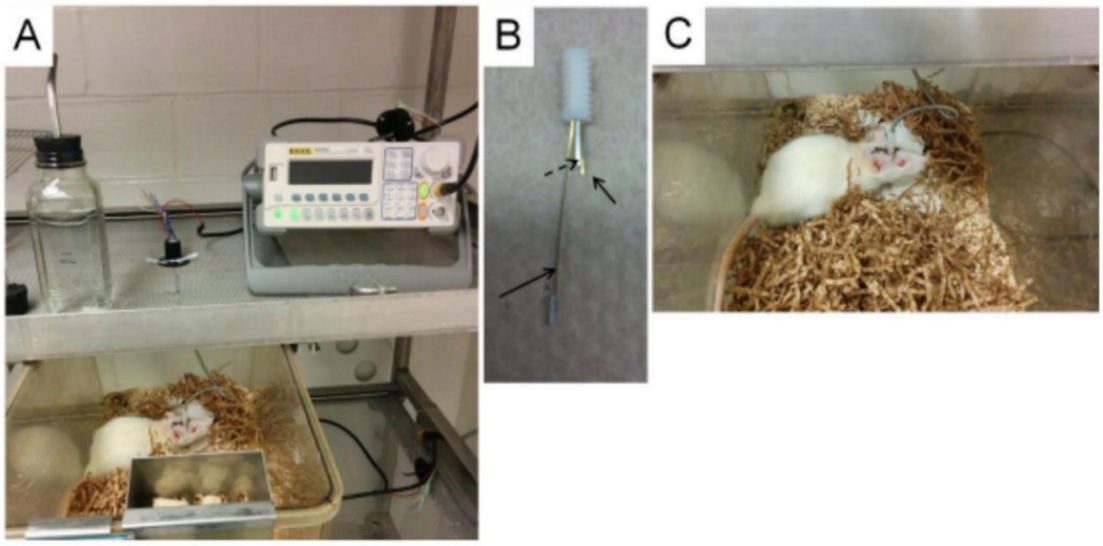

Figure 4. In vivo IMT apparatus.

Four days after stereotactic bilateral tumor implantation (see Figure 6) animals were unilaterally treated with continuous IMT (frequency: 200 kHz, amplitude: +/- 2V) for seven days. The contralateral tumor acted as an intra-animal sham control and did not receive treatment. A) Electrical stimulation was produced by a waveform generator connected to an implanted electrode in the rat brain. A flexible commutator connects the electrodes and waveform generator and permits free movement throughout the cage. B) A representative cannula electrode construct to be bilaterally implanted into the striatum. The construct is composed of a cannula (dashed arrow) and adjacent electrode (short solid arrow), allowing for F98 cell injection followed by stimulation at the epicenter of the tumor. A reference electrode (long solid arrow) is implanted outside the skull within the nuchal soft tissues. C) Closer view of the animal undergoing IMT.

2.4 Brain Extraction and Tissue Sectioning

Rats were euthanized 4, 7, or 11 days post-surgery. Following an intraperitoneal injection of Euthanyl (~0.3 mL, Bimeda, Cambridge, ON), animals were perfused trans-cardially with 0.9% saline for 3 minutes, and subsequently with 4% paraformaldehyde (PFA) for approximately 7 minutes. Brains were removed and post-fixed in 4% PFA for one hour at 4°C before they were then transferred to 30% sucrose for approximately three days. Brains were sliced in 16µm coronal sections with a Leica cryostat and directly mounted onto charged slides (Fisher Scientific, Ottawa, ON).

2.5 Thionin Staining

To prepare the tissue for thionin staining, slides were baked at 37°C for 30 minutes, rinsed in 0.1M phosphobuffer saline (PBS) for 15 minutes, and then baked at 60°C for one hour. The slides were then cleared in xylene overnight. Next, the slides were transferred to propanol for 30 minutes, followed by rehydration by two minutes each in 100, 96, 90, 70, and 50% ethanol. The slides were then transferred to distilled water for five minutes, and then stained in thionin for 20 seconds. After rinsing the slides in distilled water, the slides were dehydrated by submerging them for two minutes each in 50, 70, 90, 96, and 100% ethanol. Slides were subsequently differentiated in a solution of 1mL glacial acid and 250 mL ethanol for 10 seconds, before being transferred to 100% ethanol for three minutes, twice. Slides were then transferred to a 1:1 mixture of terpineol and xylene for 15 minutes, and then transferred to xylene for 15 minutes, twice. Slides were then cover-slipped (Fisher Scientific, Ottawa, ON) using entellan mounting media (EMD Millipore, Billerica, MA).

2.6 Immunohistochemistry

Slides were heated at 65ºC for 20 minutes and washed in 0.1M PBS three times for 5 minutes each to wash off excess cryoprotectant. Slides were permeabilized with 2.5% TritonX-100 (Calbiochem, Etobicoke, ON) for 45 minutes and washed 3 times with PBS. Slides were incubated in a blocking solution (1% Bovine Serum Albumin, BSA EMD Millipore, Billerica, Massachusetts in PBS) for one hour followed by incubation in Rabbit-anti-cleaved caspase-3 (1:33, Cell Signalling, Danvers, MA) diluted in 1% BSA overnight at 4ºC. Slides were washed with PBS and incubated in AlexaFluor Goat-anti-rabbit 546 (1:100, Life Technologies, Grand Island, NY) for 1 hour in the dark. Slides were washed three times in PBS, and counterstained with 4'-6-diamidino-2-phenylindole (DAPI; 1:1000 in PBS, Life Technologies, Grand Island, NY) for 5 minutes. Slides were washed three times in PBS and coverslipped with Prolong Gold Antifade reagent (Life Technologies, Grand Island, NY). Slides were allowed to dry and then sealed with nail polish.

2.7 Brain Tissue Imaging

Slides were imaged with a Nikon Eclipse Ni-U upright microscope with an attached DS-Fi2 high-definition colour camera and imaging software (Nikon Imaging Software-Elements), and NIS-Elements colour camera (Nikon Instruments, Melville, NY).

2.8 Stereological Analysis

A quantitative measurement of tumor size and surface area was obtained using the Cavalier estimator on Stereo Investigator software (MBF Bioscience, Williston, Vermont) attached to a Nikon Eclipse 90i microscope (Nikon Instruments, Melville, NY). Section thickness and number of series per section were input into the program to

calculate length between sections. A blinded operator delineated tumor margins rostral to caudally to encompass the entire sham and treated tumors. Each tumor outline was then merged to generate a three-dimensional (3D) visual representation of the two tumors, and a measurement of tumor volume and surface area **(Figure 5)**.

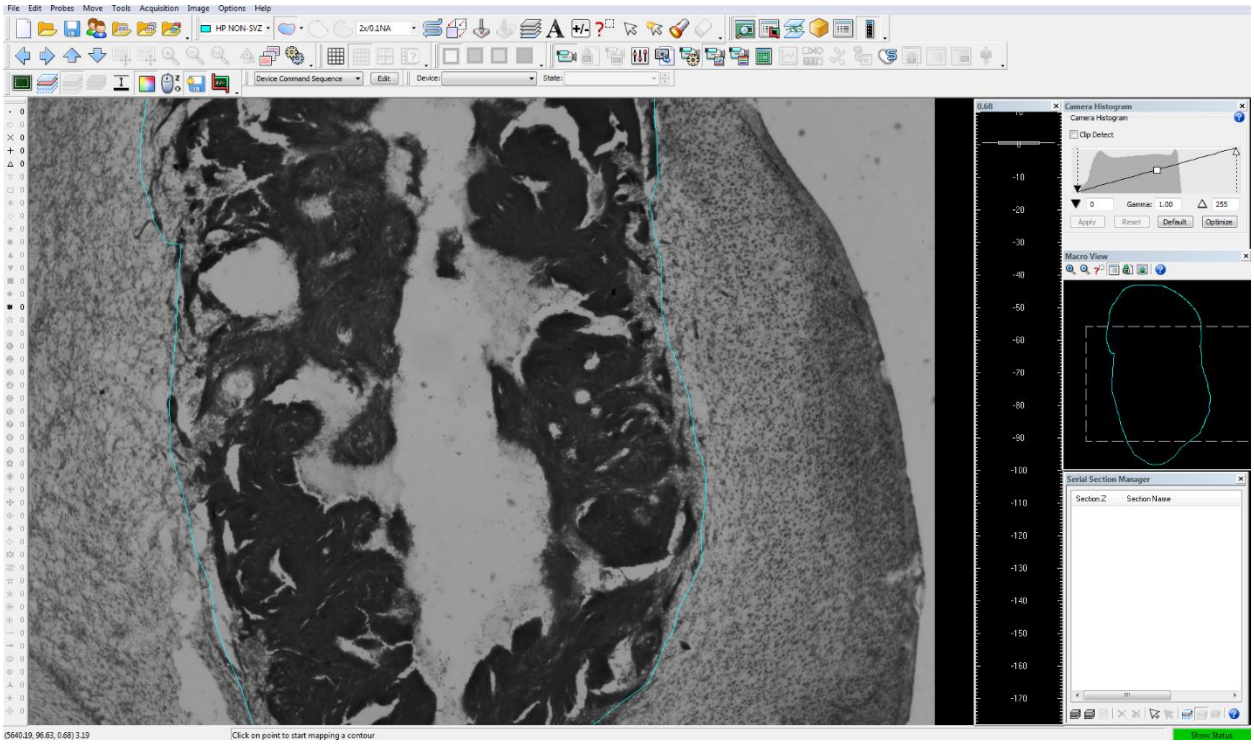

Figure 5. Stereo Investigator software.

A representative section of a tumor undergoing quantification using the Stereo Investigator software. The tumor margins of both sham and treated tumors were highlighted by a blinded operator. Once the tumor margins for both tumors were completely delineated rostral to caudally, the program merged all outlines into 3D representation of the tumors. Using the number of sections highlighted, and section thickness, the program calculated an approximate surface area and volume for both the treated and control tumor.

2.9 Bioluminescent Imaging

Approximately 20,000 F98 cells were transduced with a pre-made commercial lentivirus, Redifect Red-Fluc-GFP (Perkin-Elmer, Waltham, MA) at a multiplicity of infection of 50. Transduction was mediated by the viral transfection agent polybrene (EMB Millipore, Billerica, MA). After 24 hours of cell growth the media was replaced with fresh medium. Following 48 hours of growth, the cells were thoroughly washed with PBS and then suspended using TrypLE (Fisher Scientific, Ottawa, ON). The cells were passaged several times, and then sorted twice using fluorescence activated cell sorting (FACS) to isolate the highest GFP expressing cells. Sorted cells were pre-stained with 7-aminoactinomycinD (7AAD) to permit dead cell exclusion. Selected cells were then prepared as previously described for striatal injection.

All *in vivo* bioluminescent imaging (BLI) was performed using a hybrid optical/X-ray scanner In Vivo FX Pro (Bruker Corporation, Billerica, MA). Rats were anesthetized with 5% isoflurane and 2% oxygen, and maintained under anesthesia in the scanner with a secured nose cone. On days 4, 7, and 11 after surgery rats received 1 mL of the luciferase substrate, D-Luciferin, intraperitoneally, and whole body BLI images were captured for up to 30 minutes. A signal intensity map, generated by measuring photons emitted per second per square millimetre, was used to quantify bioluminescent signal. The intensity map was created at every time point to produce a quantifiable visual metric for tumor progression.

2.10 Magnetic Resonance Imaging

Imaging at 7 days was performed using a 9.4T small-animal magnetic resonance imaging (MRI) scanner (Agilent, Santa Clara, CA). Rats were injected with gadolinium intraperitoneally 15 minutes before they were sacrificed, and perfused following the previously mentioned protocol. The rat was then imaged. Rats were setup in a custom built MRI compatible cradle, and images were acquired using a custom built radiofrequency surface coil. The 3 scans acquired were a 2D fast spin echo (FSE) sequence, a 3D Flash sequence, and a 3D True FISP sequence. The 2D FSE sequence had voxel size 38.4mm by 38.4mm, matrix size 41mm by 0.5mm, TR = 3 seconds, TE = 50 ms. Flash 3D sequence had voxel size 28mm by 20 mm by 28mm, matrix size 140 mm by 140 mm by 140 mm, flip angle = 25°, TR = 40ms, TE = 6ms. 3D True FISP sequence had voxel size 28mm by 28 mm by 28mm, matrix size 140 mm by 140 mm by 140mm, flip angle = 30°, TR = 7ms, TE = 3.5ms.

2.11 Statistical Analysis

SPSS was used for statistical analysis. Data are expressed as group means ± the standard error of the means. Student's one-sample t-tests was used to assess significant differences between groups. * indicates statistical difference between group means ($p<0.05$).

PART 3: RESULTS

Results

3.1 Tumor progression of F98 gliomas in Fischer rats

To assess tumor size at commencement of IMT, animals underwent unilateral stereotactic implantation of 40,000 F98 cells into the caudate putamen. Separate animals were sacrificed after 4 days of tumor growth, at the time when IMT would begin, as well as on day 7 and on day 11. Tissue histology revealed robust tumor growth at day 4, with invasion into the surrounding brain parenchyma. Tumor size greatly increased by day 7, and at day 11 the tumor covered almost the entire area of the caudate putamen. These results indicate that IMT is delivered to already robust tumors.

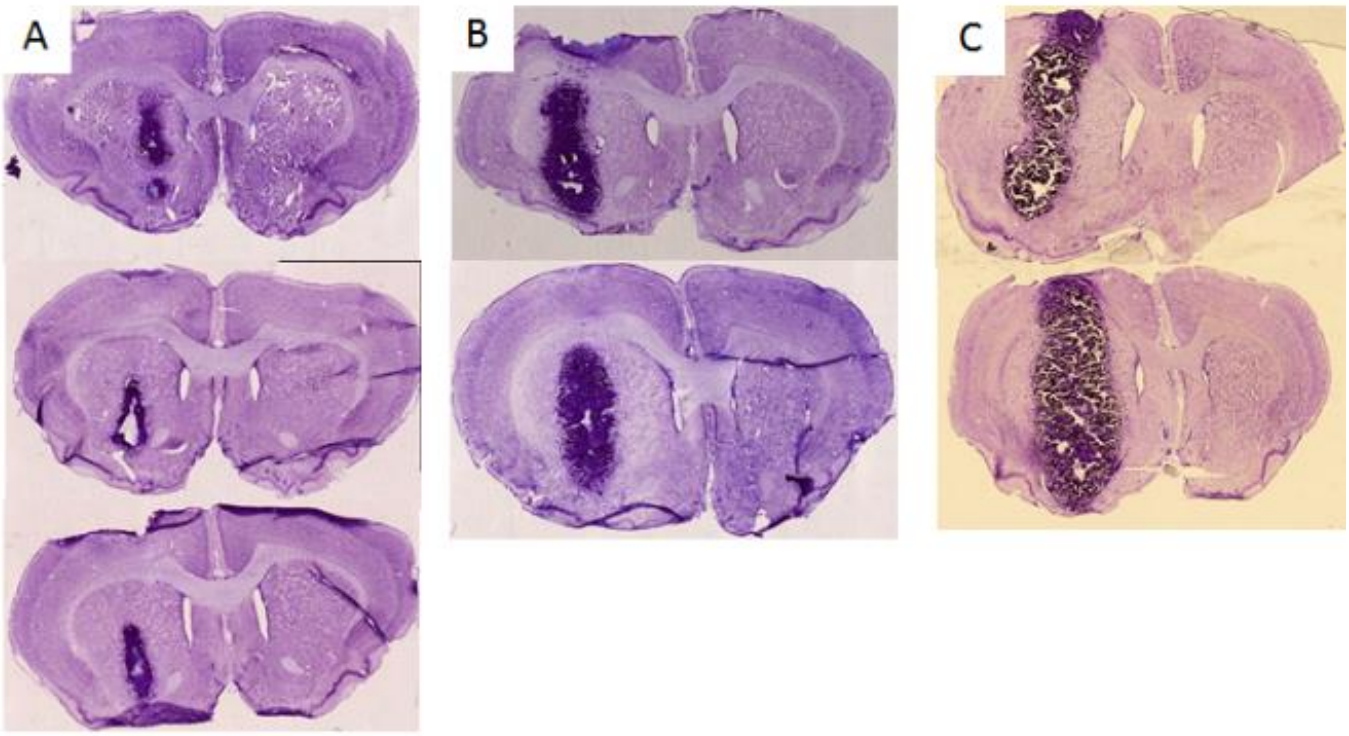

Figure 6. Tumor progression of F98 gliomas.

Thionin stained brain tissue slices 4, 7, and 11 days following a unilateral striatal injection of 2µL of PBS containing 40,000 F98 cells. The tumors are highly aggressive and proliferative and appear dark purple due to their high cellular density compared to normal parenchyma. A) Representative thionin stained sections following 4 days of tumor growth in three different rats. B) Representative thionin stained sections following 7 days of tumor growth in two different rats. C) Representative thionin stained sections following 11 days of tumor growth in two different rats. Widespread necrosis is visible within the tumors at 11 days.

3.2 IMT attenuates F98 tumor growth

To model IMT, adult Fischer rats underwent bilateral implantation of cannula electrode constructs and were injected bilaterally with 40,000 F98 cells into the caudate putamen. At day 4 post-surgery one electrode was attached to the waveform generator, while the other acted as a sham control. The waveform generator delivered IMT at a frequency of 200 kHz and amplitude of +/- 2V for 7 days continuously. After 7 days, the rats were sacrificed and their brain tissue was collected and analyzed to determine the effect of IMT. Thionin staining revealed a dramatic difference in tumor size between the untreated and IMT treated tumors **(**n=10, **Figure 8)**. Treated tumors appeared larger in size than tumors stained 4 days post-surgery, yet smaller than tumors stained 7 days post-surgery, indicating a therapeutic inhibitory effect on glioma cell growth.

When these experiments were conducted, the model was continuously improved and refined to increase the reliability of IMT **(Table 1)**. From the animal represented in **Figure 8G** and onwards, a strict troubleshooting protocol was followed to account for potential pitfalls that may have limited IMT efficacy and reproducibility. Before surgery, the entire apparatus used to generate IMT was assembled, and an oscilloscope was used to measure waveform frequency from the cannula electrode tip. This ensured no component parts were defective, and the cannula electrode would be able to deliver stimulation after implantation. During all 7 days of stimulation, an oscilloscope was used to measure waveform frequency directly from the waveform generator output port. After the animal was euthanized, the cannula electrode was extracted from the rat scalp and plugged back into the apparatus. The entire apparatus was then re-measured with an oscilloscope to ensure the electrode was not damaged during the week of treatment. As

well, the animal must survive to the end of the time point, and the apparatus must be able to deliver stimulation before, during, and after IMT for the animal to be classified as receiving the full treatment. After developing these quality control checks, a run of 10 straight animals received IMT, and then had stereological analysis performed on their tumors. Three animals from the group were excluded from analysis: one animal died after surgery, and two animals did not receive consistent stimulation deemed adequate to represent the effects of IMT. From the remaining animals, histological analysis revealed morphological changes in IMT treated tumor shape and size **(Figure 9)**.

A stereological volume and surface area estimator was used to obtain a quantitative measurement of tumor size for all 7 remaining animals in the cohort, which revealed a significant decrease in treated tumor surface area and volume when normalized to their sham controls (Volume: $t=7.662$, $df=6$, $p=0.0001$). There was no significant decrease in surface area or volume in treated tumors when comparing raw data, although there a trend was present (Volume: $t=1.775$, $df=6$, $p=0.063$; Surface Area: $t=1.795$, $df=6$, $p=0.0615$). Representative 3D models of tumors within the brain parenchyma were generated to show the bilateral tumor dimensions of a typical responder and non-responder to treatment **(Figure 10).**

Table 1. Animals used in the study to date

Experiment	Total animals used	Experiment successful	Experiment unsuccessful	Reason for failure
IMT	n = 35	n = 10	n = 25	*n = 14* (inviable cells did not grow robust tumor) *n = 5* (rat died during surgery) *n = 3* (rat chewed through commutator connection disrupting stimulation) n = 3 (rat did not respond to treatment)
No stim control	n = 3	n = 3		
4 day control	n = 9	n = 3	n = 6	*n = 6* (inviable cells did not grow a robust tumor)
7 day control	n = 7	n = 3	n = 4	*n = 4* (inviable cells did not grow a robust tumor)
BLI	n = 2	n = 1	n =1	*n = 1* (tumor grew, but BLI signal did not appear)
MRI	n = 6	n = 1 (IMT only for 4 days) n = 1 (7 day tumor imaging) n = 2 (11 day tumor imaging)	n = 2 (7 day tumor imaging)	*n = 2* (inviable cells did not grow a robust tumor)

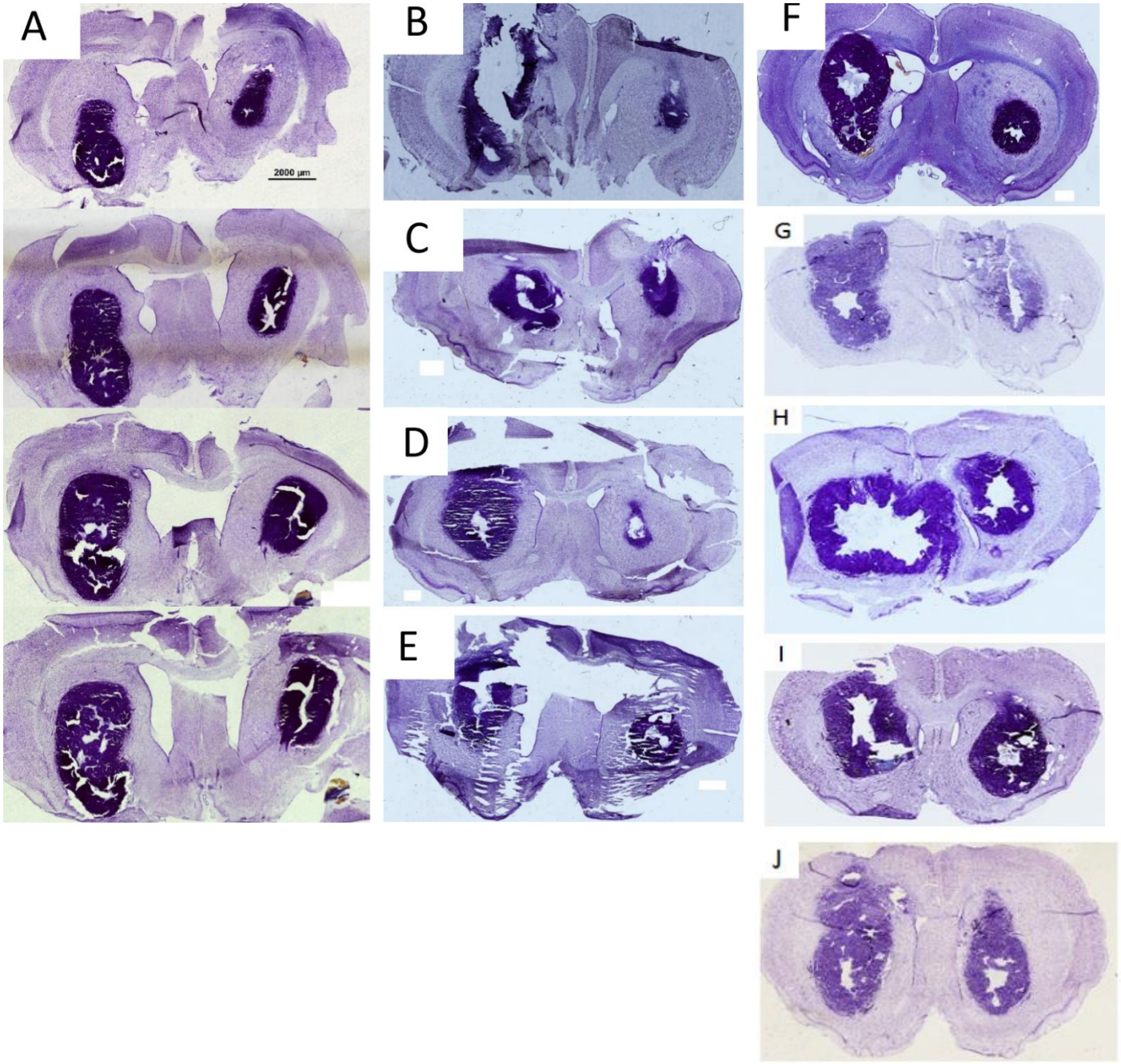

Figure 7. IMT impedes tumor growth in the F98 glioma model.

Photomicrographs of Fischer rat brain slices treated with sham conditions (left tumor) or IMT (200kHz, +/-2V) for 7 days (right tumor). A) Sample rostral to caudal sections show a dramatic difference in tumor size between treated and untreated tumors. B-J) Representative sections each from a different animal that received IMT demonstrated a marked reduction in tumor growth on the treated side. A rigorous quality control protocol was developed over the course of experimentation and fully implemented from brains G-J.

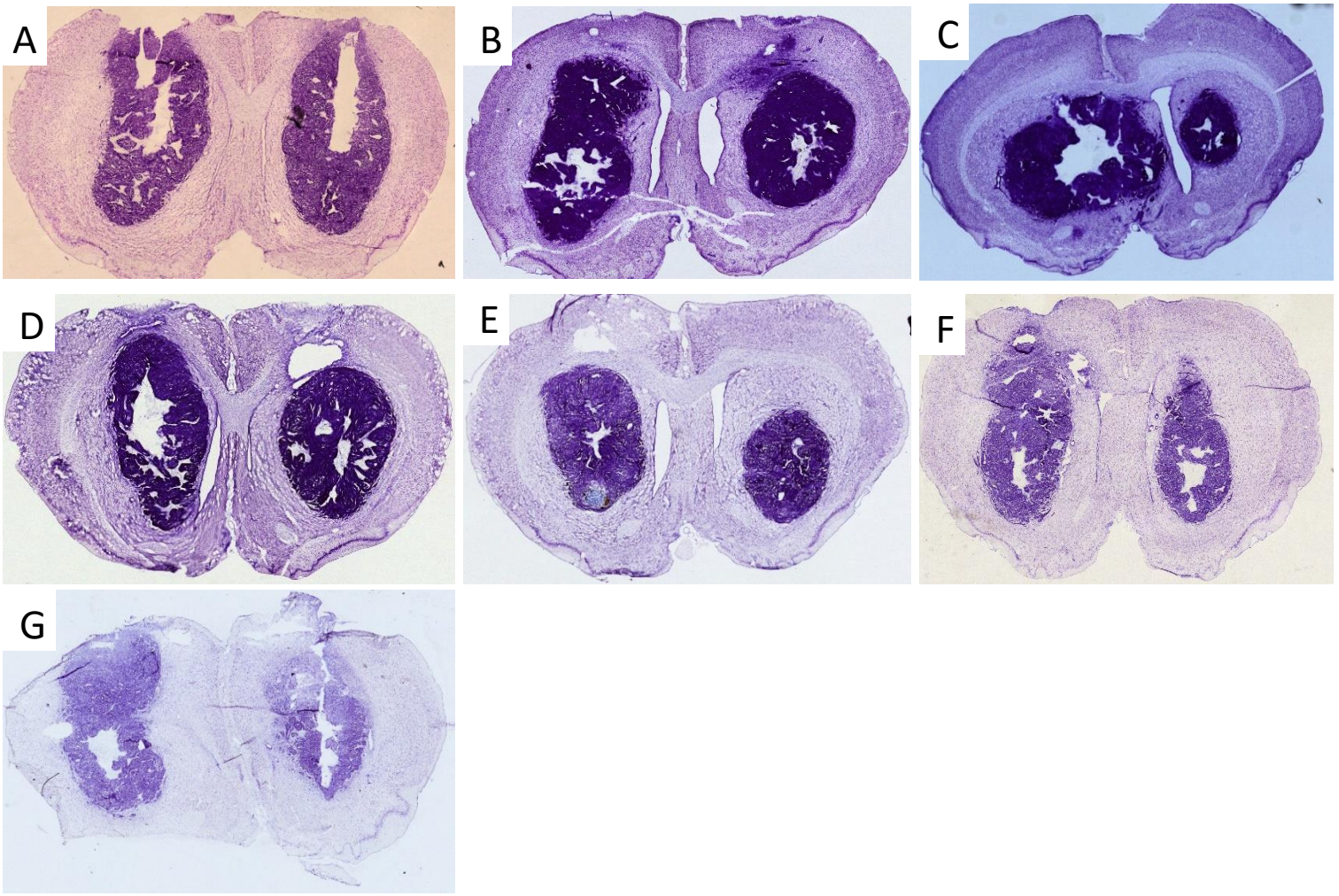

Figure 8. IMT cohort of 10 consecutive animals

A-G) Representative photomicrographs of the 7 animals deemed suitable for analysis after undergoing 7 days of IMT. Tumors on the right received IMT at previously mentioned parameters, while tumors on the left acted as a sham internal control. All animals were processed with the same quality control protocol to ensure maximal IMT reliability. Each animal responded differently to the treatment, although A,B, and D appeared to have marginal to no effect.

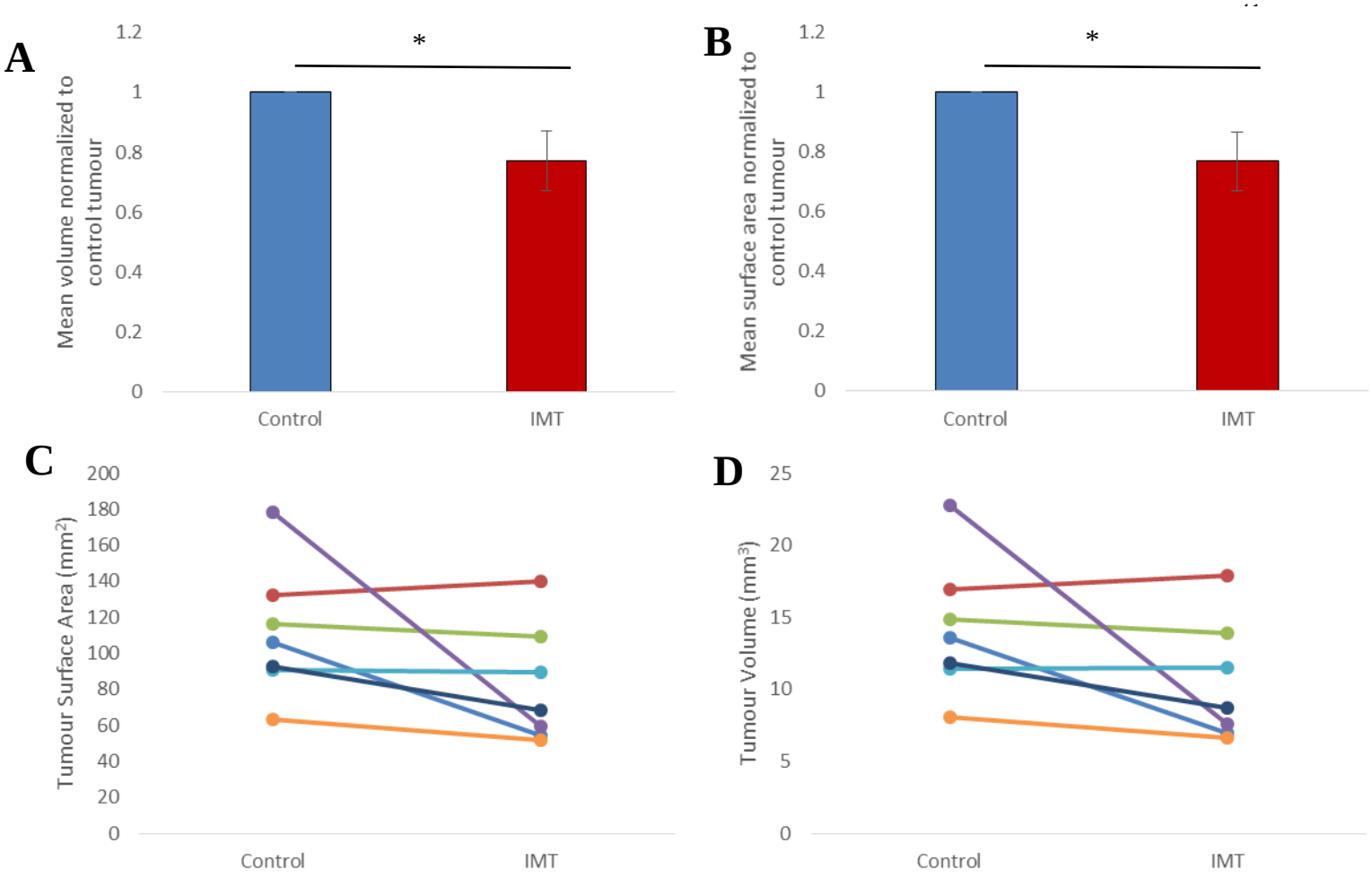

Figure 9. IMT significantly reduces treated tumor area and volume relative to its sham control.

The n=7 animals from **Figure 9** underwent stereological analysis to quantitatively measure control and treated tumor surface area and volumes. A,B) Histograms reveal a significant decrease ($p=\leq 0.0001$, $p=\leq 0.0001$) in both surface area and volume for IMT treated tumors normalized to their sham controls. C,D) Line plots reveal no significant difference between control and treated tumor surface area and volume, although a trend is present ($p=0.0615$, $p=0.063$). Normalized data for surface area and volume were compared using a one-tailed, one-sample t-test, and raw data were compared using a one-tailed paired t-test. Significance is denoted with a * and was chosen to be $p<0.05$. No data were found to be outliers (classified as 3 standard deviations away from the mean).

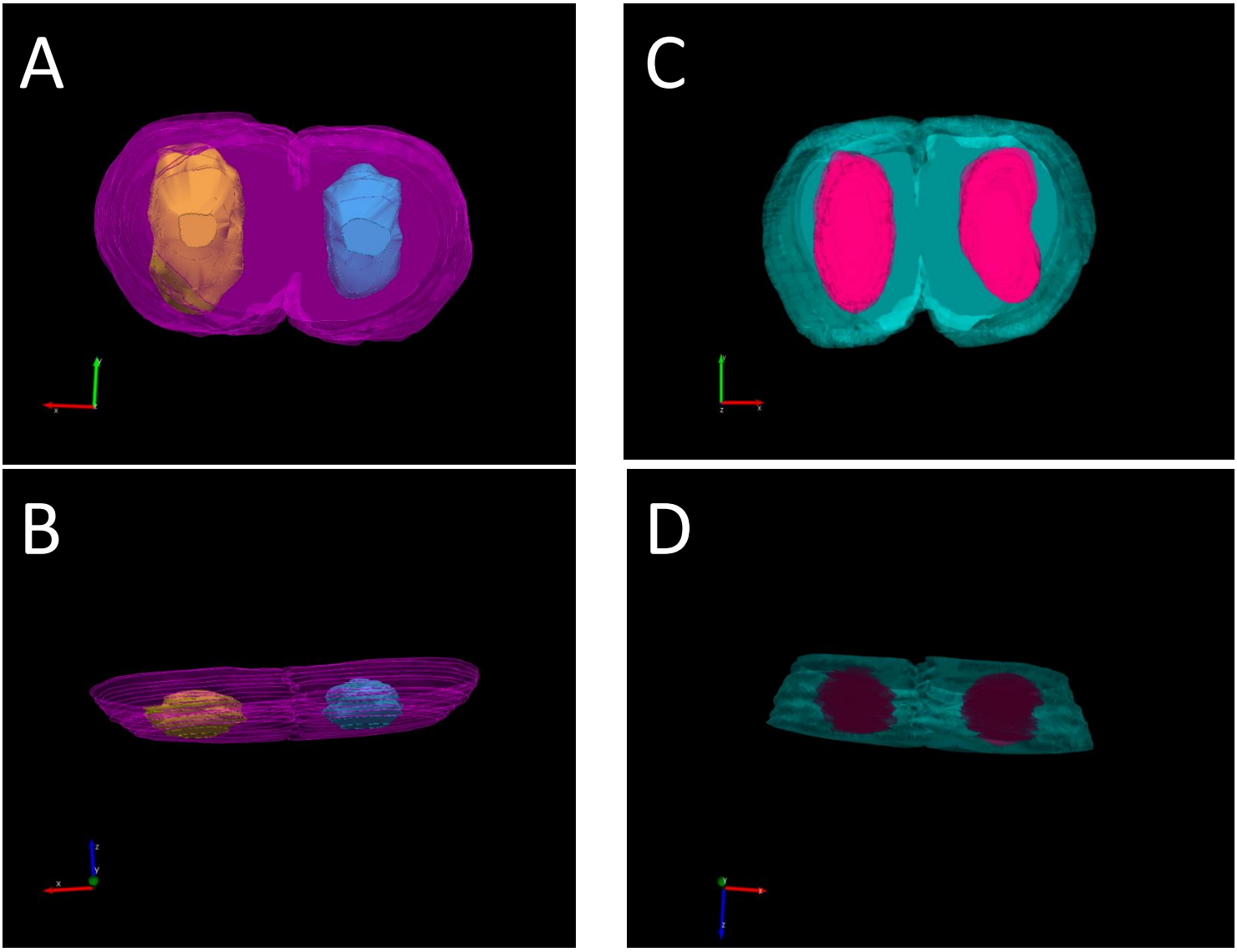

Figure 10. 3D modelling of IMT F98 glioma tumors.

A) Coronal, and B) axial view of a representative responder within the cohort of 10 animals. The IMT treated tumor is on the right, and is visibly smaller than its control

counterpart. C) Coronal, and B) axial view of a representative non-responder within the tested cohort. Both tumors appear to be the approximately same size.

3.3 IMT does not change histology of normal brain parenchyma

Another group of rats received the same bilateral implantation of cannula electrode constructs, but did not have any tumor cells implanted. However, these rats were stimulated before the rigorous quality control steps were developed and implemented. After four days of recovery after surgery, IMT was delivered unilaterally to each rat for 7 continuous days directly to the normal brain parenchyma **(Figure 11)**. Tumor histology show no notable defect on the IMT treated side compared to the control.

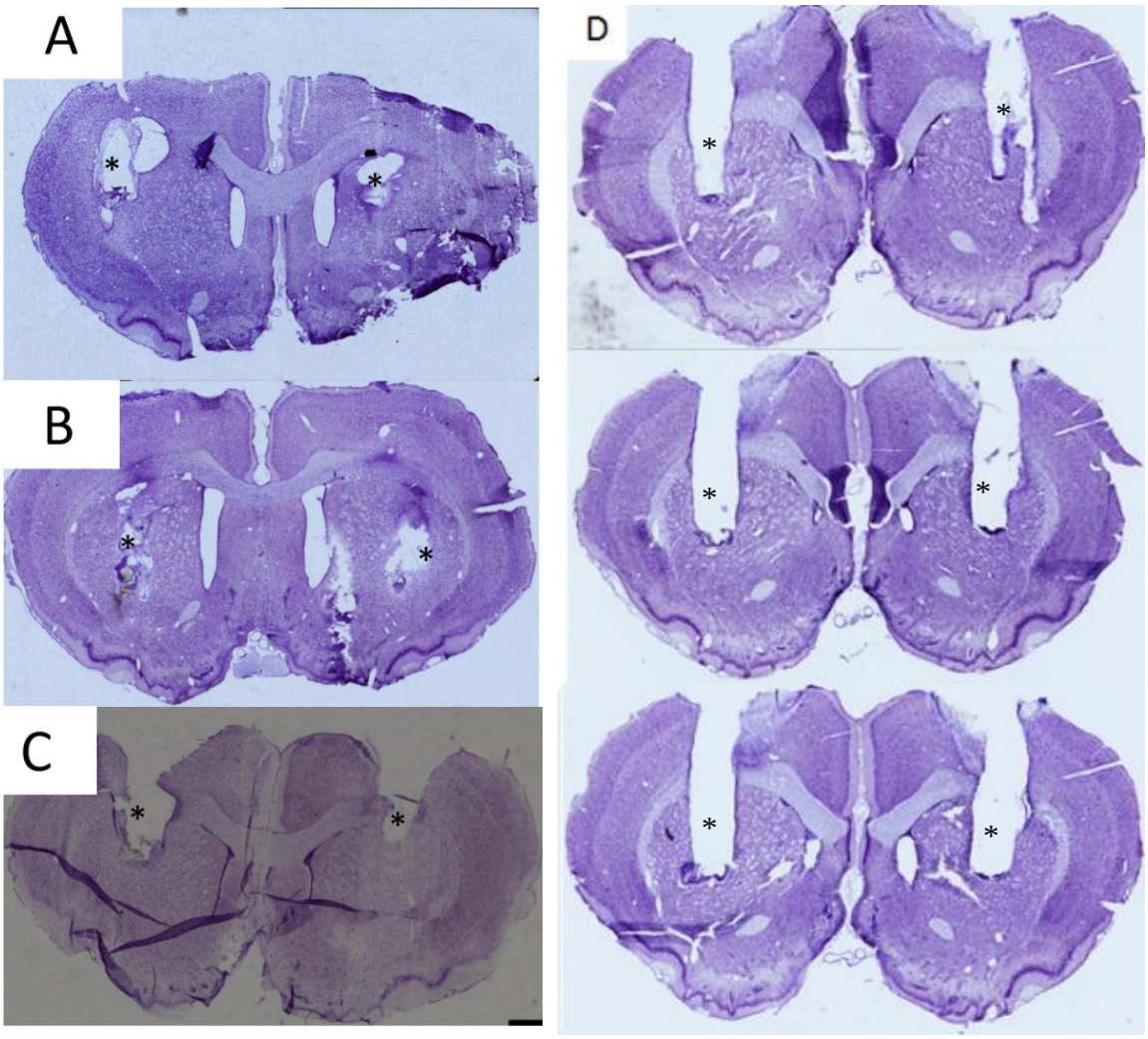

Figure 11. IMT in normal brain parenchyma.

A-C) Three different control animals received bilateral cannula electrode construct implants, but no tumor cell injections and were unilaterally stimulated. D) Rostral to caudal slices of a rat with bilateral implants, but unilateral stimulation. For all animals, sham conditions are pictured on the left, and electrical stimulation with the same parameters as IMT on the right. Asterisks indicate hardware defect caused by the implanted constructs; however, there was no notable injury to normal brain parenchyma in IMT treated tissue compared to the sham control.

3.4 Cleaved caspase-3 expression in IMT treated tumors

Immunohistochemical staining for cleaved caspase-3 revealed expression in the core of both the IMT treated and control tumors, but a higher overall expression in the IMT treated tumor **(Figure 12)**. However, this pattern of expression was not consistent with all treated animals. Cleaved caspase-3 was also heavily expressed in the necrotic core of both IMT treated, and control tumors **(Figure 13)**. Activation of caspase-3 to cleaved caspase-3 is a key step in apoptosis, and the presence of cleaved caspase-3 is used as a marker to indicate the occurrence of cellular apoptosis. Immunohistochemistry without the primary antibody did not reveal any non-specific staining **(Figure 14)**.

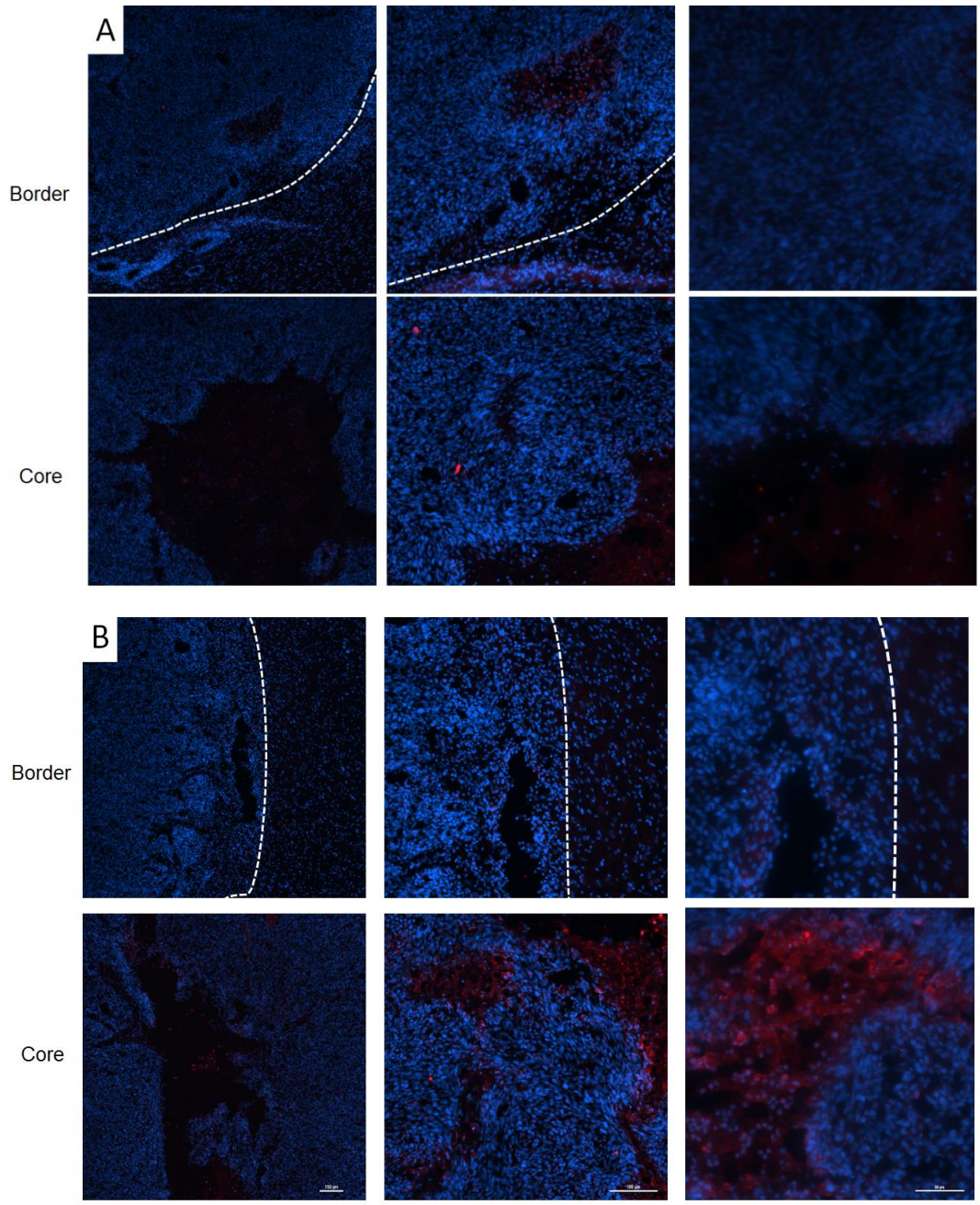

Figure 12. IMT initiates caspase-mediated apoptosis

A) Non-treated tumor shows little cleaved caspase-3 activity (red) at the tumor border,

but increased expression in the core. B) Likewise, the treated tumor from the same animal shows little cleaved caspase-3 at the tumor border, and increased cleaved caspase-3 expression. Staining for cleaved caspase-3 was highest near the centre of both tumors. Cleaved caspase-3 signal was much higher in treated tumour than non-treated tumour. The dotted white lines delineate the tumor border and beginning of normal parenchyma.

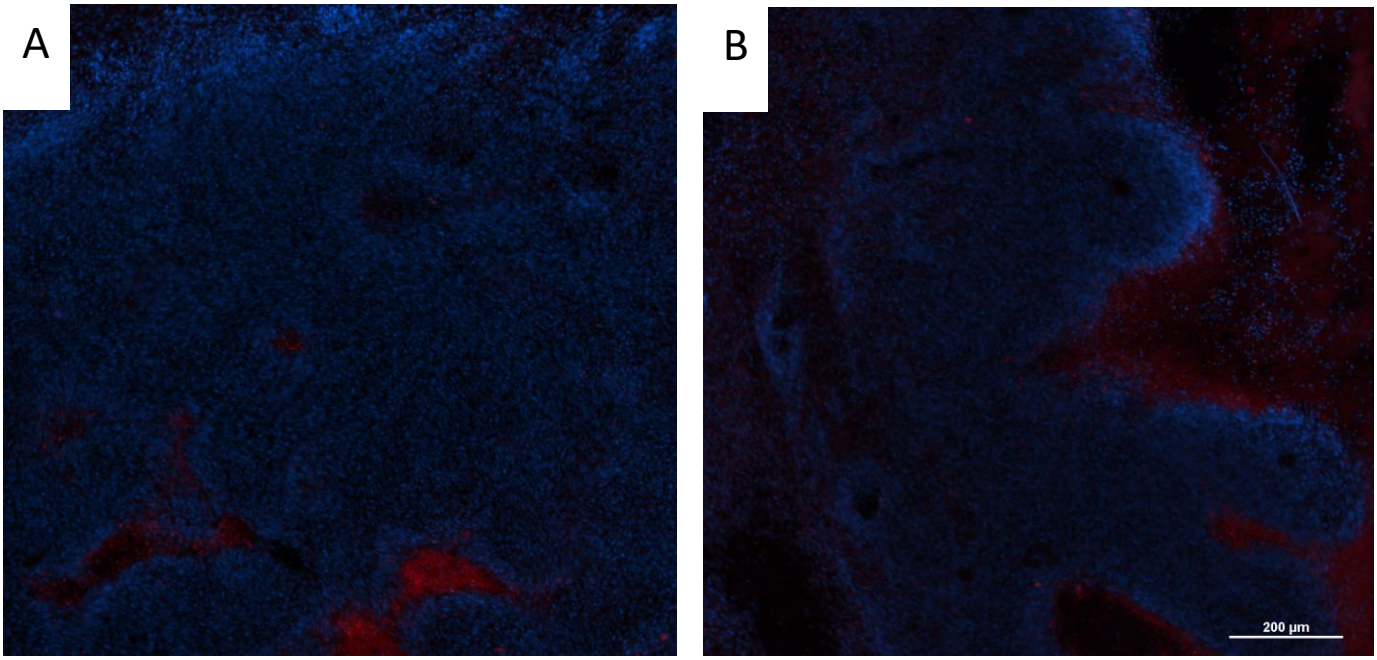

Figure 13. Cleaved caspase-3 expression non-specifically found in tumor core

A) Non-treated tumor shows elevated cleaved caspase-3 activity at the tumor core (bottom of image). B) Likewise, treated tumor shows elevated cleaved caspase-3 expression at tumor core.

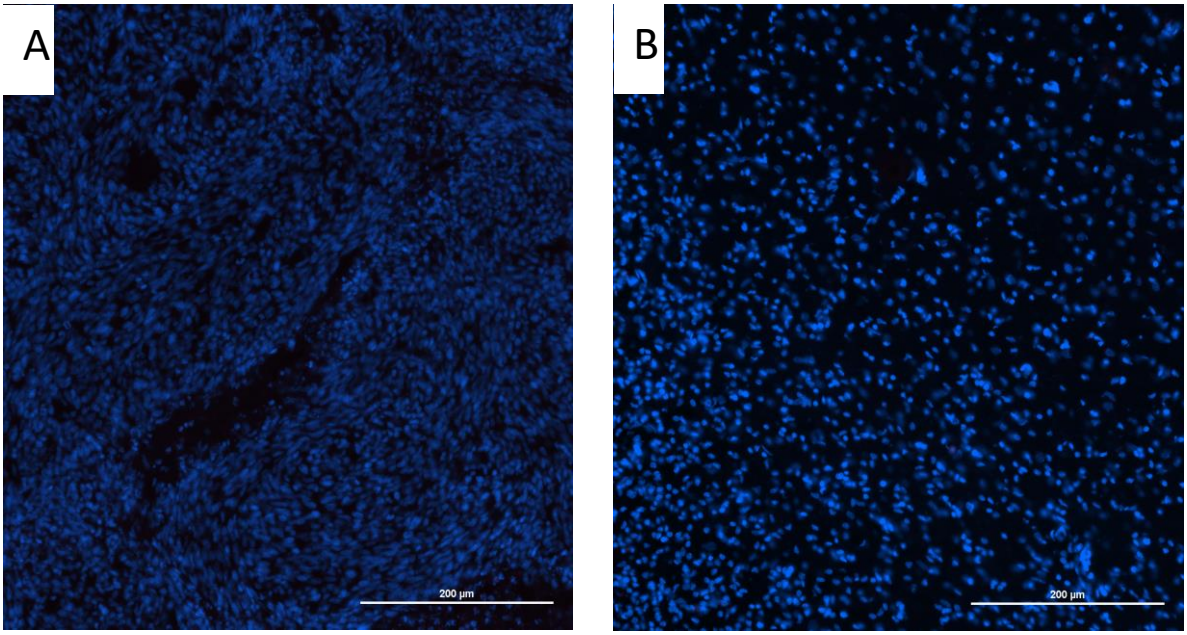

Figure 14. Cleaved caspase-3 antibody exhibits little non-specific binding

Staining with no primary antibody for cleaved caspase-3 showed little to no caspase activation in both A)sham and B)IMT tumors demonstrating secondary antibody specificity. Treated tumor was stimulated with IMT for 7 continuous days.

3.5 Multi-modal imaging to non-invasively track tumor progression

A pair of animals were injected with F98 cells transfected with the bioluminescent gene firefly luciferase. Bioluminescent imaging was chosen as an imaging modality, because it is non-invasive, relatively inexpensive compared to other modalities, and easy to reproduce. After 4 days of tumor growth, at the time when IMT would begin, as well as day 7 and 11, animals underwent bioluminescent imaging if applicable and were then sacrificed. Tissue histology and bioluminescent imaging both revealed robust tumor growth, with invasion into the surrounding brain parenchyma (**Figure 6,15)**. These results indicate that IMT is delivered to already robust tumors, and demonstrate the ability to non-invasively measure tumor burden and progression.

A pilot MRI study was conducted to refine the tumor imaging procedure and observe tumor size at day 7 and 11 (**Figure 16)**. Tissue histology was correlated with MRI scans at 7, and 11 days to provide more comprehensive modelling of tumor size and shape at each time point**(Figure 6)**.

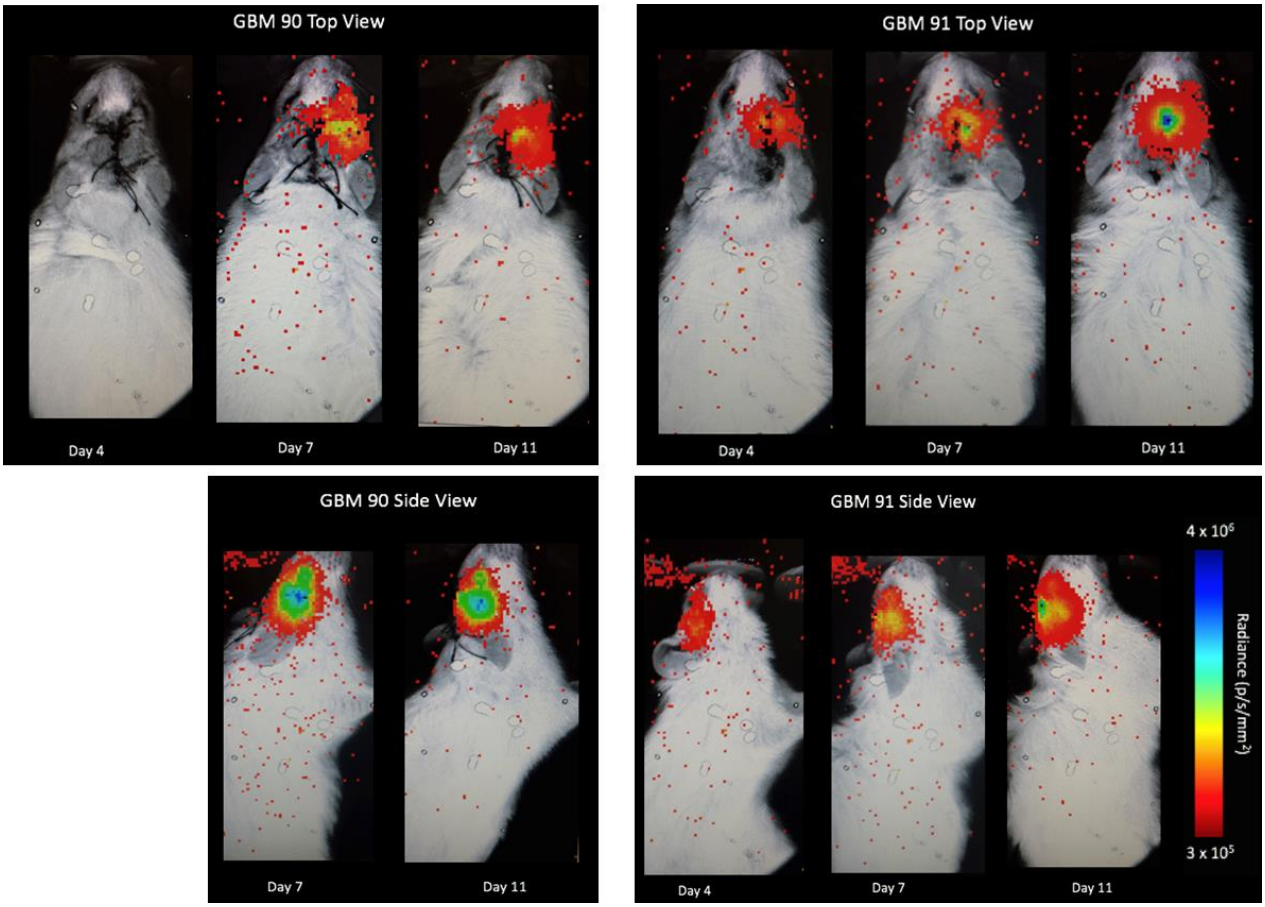

Figure 15. Bioluminescent imaging of F98 gliomas.

Bioluminescence imaging (BLI) of two Fischer rats 4, 7, and 11 days after a unilateral striatal injection of 2µL of PBS containing 40,000 F98 cells. The BLI signal is concentrated in the region of cell injection, and robust. BLI signal strength dramatically increases in intensity over the course of the 11 day period. p/s/mm^2; photons, per second, per millimetre squared

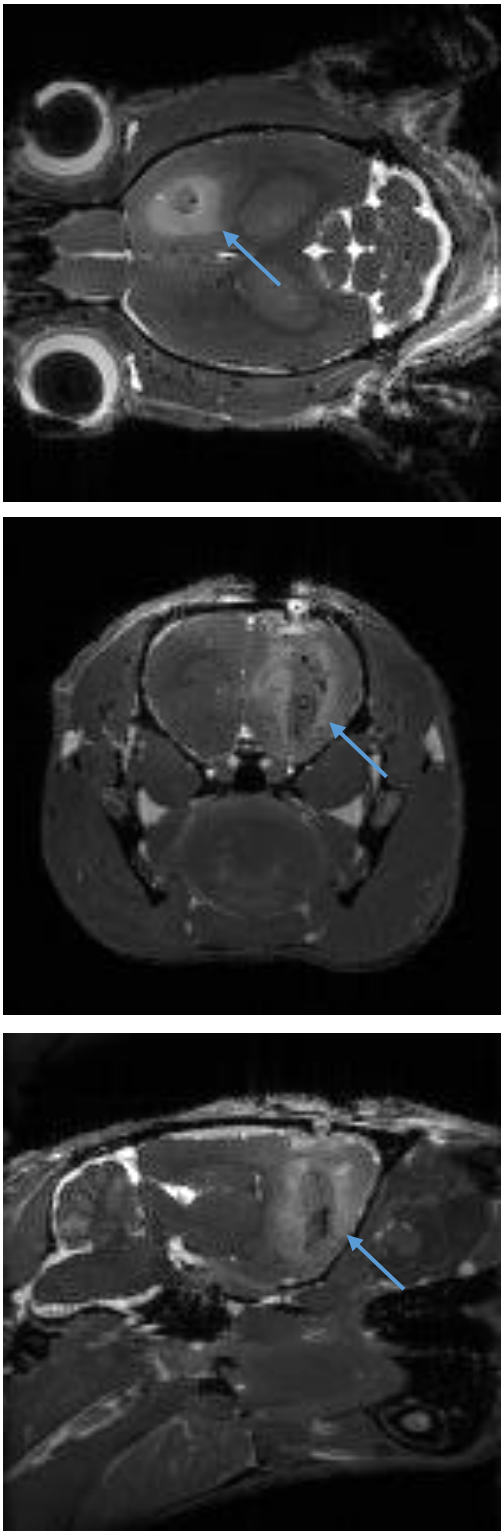

Figure 16. MRI of an F98 glioma after unimpeded glioma growth 7 days post-surgery

T2 weighted MRI image of Fischer rat brain 7 days after unilateral deposit of 40,000 F98 cells. The rat was sacrificed before imaging, and the brain tissue was harvested immediately after the MRI scans. Top to bottom images show axial, coronal, and sagittal images of the tumor respectively. Arrows point to substantial peritumoral edema surrounding the tumors.

PART 4: DISCUSSION

Discussion

IMT has shown promise as a potential treatment for GBM *in vitro*. Establishing an animal model of IMT is a necessary preclinical step before it may be used in humans. Here, we established a proof of principle model of IMT in the Fischer rat, and evaluated the efficacy and safety of the treatment. We observed a significant reduction of tumor surface area and volume in tumors treated continuously for 7 days compared to their sham controls. In addition, we found treated tumors had increased expression of markers for cell death relative to their sham tumor counterparts. We also visualized tumor progression using bioluminescent imaging and magnetic resonance imaging, which may be used in the future to non-invasively evaluate the treatment effect of IMT.

4.1 Assessing tumor progression of F98 gliomas in Fischer rats

In this study, we found that 40,000 F98 cells injected into the caudate putamen of a Fischer rat generated robust tumors only 4 days after injection, and the tumors rapidly and aggressively grew throughout the 11 day timeline. The F98 Fischer rat glioma model used in this study was based on an established protocol by Mathieu et al, and chosen because of its reproducibility and similarity to human GBM(Mathieu et al., 2005, 2007).

Our first experiments were to assess the progression of the tumor without IMT stimulation and therefore no cannula electrodes were implanted. Instead, the rats were unilaterally injected with F98 cells through Hamilton syringes. The purpose of evaluating tumor histology at 4,7, and 11 days was to ensure tumors grew reliably and at a consistent rate throughout the experimental timeline, and determine tumor size at the start of IMT, 4 days post-surgery. Our data showed that there is substantial tumor growth at 4 days post-

surgery, and a clear progression of tumor size at 7 and 11 days post-surgery. At the three evaluated time points, tumor borders were diffuse and appeared to infiltrate into the surrounding parenchyma.

Studies using the same surgical protocol for the F98 glioma model found similar results, although only 10,000 cells were injected so tumor burden was smaller at comparable time points(Blanchard et al., 2006). Assessing tumor histology at the 4 day post-surgery time point was particularly important, because it marked the initiation of IMT in treated animals. Although the 4 day tumor was relatively small compared to its 7 and 11 day counterparts, it still represents a sizable tumor mass. Therefore based on corresponding histology, IMT in the following experiments was delivered to an already existing tumor mass, and not a small deposit of cells. This is more clinically analogous to delivering IMT to a tumor mass, rather than an already resected tumor bed.

4.2 Delivering IMT to normal brain parenchyma

IMT delivered for 7 continuous days to normal brain parenchyma did not appear to cause any tissue damage. The tissue receiving IMT showed no signs of necrosis, bleeding, edema, or other damage compared to a sham control within the same brain. This suggests that IMT does not have an injurious effect on non-cancerous brain tissue. However, these experiments were performed before the rigorous quality control steps were developed and implemented, and therefore should be repeated with the aforementioned steps in place.

These findings correlate with previously performed *in vitro* experiments, which showed no change in embryonic rat neuronal cell viability after 72 hours of exposure to IMT **(Figure 2)**. In this experiment, we performed bilateral cannulation of the cannula

electrode construct in Fischer rats following the same protocol as our IMT experiments, but crucially we did not inject F98 cells through the cannulas. We then replicated the treatment protocol for IMT, delivering unilateral stimulation (sine wave, 200 kHz, +/- 2V) 4 days after surgery for 7 continuous days, directly into normal brain parenchyma.

For comparison, a similar study investigating electrochemotherapy in a rat glioma model intratumorally delivered 8 high intensity electric pulses (100V, 0.1ms duration, 1Hz) in conjunction with 42 IU of bleomycin. The combined treatment was exceptionally effective, with 9 of 13 rats that received treatment showing no signs of tumor upon termination. To study the effect of treatment on non-neoplastic tissue, the same treatment was delivered to normal rat brain parenchyma. The electric pulses caused severe morphologic changes in the parenchyma including widespread necrosis, and a substantial loss of tissue (Agerholm-Larsen et al., 2011). Although the treatment markedly reduced tumor growth in rats, the lack of tumor specificity dramatically limits its potential use in humans.

It is critical that targeted therapies for brain tumors selectively spare surrounding normal brain tissue, especially when tumor borders are diffuse or the tumor is in an eloquent area(Pudenz, 1976). Therefore, before testing the efficacy of IMT it was important to ensure that it was indeed non-harmful to normal brain parenchyma. Overall, we conclude that IMT does not cause notable tissue damage in non-neoplastic tissue.

4.3 Evaluating the effect of IMT on tumor growth compared to internal sham controls

In this study, we found that IMT delivered continuously for 7 days significantly attenuates tumor growth compared to internal sham controls. However, the efficacy of

IMT varied between animals, ranging from a dramatic to minimal or no response to treatment. *In vitro* IMT parameters were chosen to be similar to DBS (130Hz, 4V, pulse, 50μs interval), because of the known safety of DBS in non-neoplastic tissue. However, the *in vivo* parameters were based off AEFs, because of their known anti-cancer effects, and to escape possible neuronal entrainment at lower frequency levels(Johnson & McIntyre, 2008; Kirson et al., 2004, 2007).

After bilateral cannulation and F98 tumor cell injection, tumors were allowed to grow for 4 days before initiating IMT (sine wave, 200 kHz, +/- 2V) for 7 days. As previously indicated, at 4 days post-surgery a sizable tumor mass had already grown. Nissl staining for tissue histology showed a distinct decrease in tumor size in IMT treated tumors compared to their sham controls. Treated tumors also showed a change in morphology compared to their sham controls. Sham tumors tended to grow in an elongated shape along the implanted cannula tract, whereas treated tumors maintained a rounded shape with less parenchymal invasion. It has been previously reported in the literature that regular untreated F98 tumors grow in an ellipsoid shape(Garcion et al., 2006). The change in histological tumor size and shape indicates that IMT reduces tumor proliferation and attenuates typical tumor growth, which may offer a prognostic benefit.

One of the main benefits of IMT compared to other forms of electrotherapy is the ease which stimulation can be continuously and directly delivered to the tumor-affected brain region. In contrast, AEFs must be delivered directly to the scalp for at least 18 hours a day to achieve maximal effect. In fact, a post-hoc analysis of a phase III trial for AEFs demonstrated a significantly longer median overall survival in patients undergoing treatment for over 18 hours a day (7.7 vs 4.5 months, Mrugala et al., 2014). This may

present an unacceptable burden on patients, who are responsible for the maintenance and proper usage of the device. A device delivering IMT would be completely implanted, and patients would receive therapeutic stimulation constantly without the responsibility of maintaining optimal device compliance. Therefore, a series of rigorous quality control protocols were developed to ensure IMT was continuously delivered throughout the treatment timeline. The entire apparatus used to deliver IMT was fully assembled before surgery, and the output was measured with an oscilloscope to guarantee all individual components were functional. During treatment, the output from the waveform generator was measured every day to confirm stimulation was still being delivered. Further, at the end of treatment time point, the cannula electrode was plugged back into the apparatus and re-measured with an oscilloscope to ensure the electrode was not damaged during the week of treatment. The animal must survive to the end of the time point, and the apparatus must be able to deliver current before, during, and after IMT for the animal to be classified as receiving the full treatment.

A cohort of 10 animals was treated with IMT following the aforementioned strict quality control steps, and 7 of the animals met the criteria previously set. One of the three animals died before initiation of IMT, and the other 2 animals did not meet the standards set when measuring current during IMT, and thus were discarded in the analysis. Stereological analysis on the remaining 7 rats revealed a quantifiable significant reduction in tumor volume and surface area between sham tumors and treated tumors normalized to their internal control. This indicates that IMT may indeed attenuate tumor growth in the brain. However, there were 3 non-responders in the cohort where IMT appeared to have little efficacy.

IMT's occasional lack of therapeutic effect may be explained by the stimulation area not covering the entire volume of the treated tumor. Previous studies investigating electrotherapies for cancer have shown that the entire tumor must lie within the range of the electric field or current for the treatment to have an effect (Gehl et al., 1999; Mahmood & Gehl, 2011; Miklavcic et al., 1998, 2010). Minor variations in electrode placement within the tumor, or small differences in tumor size at 4 days may have resulted in IMT's treatment effect not extending through the full extent of the tumor. Further studies should continue to develop the electrode construct used to deliver IMT, to ensure the treatment fully encompasses the tumor margins and provides a more reliable response to treatment.

4.4 The development of quality control measures and optimization of IMT

Throughout the course of this thesis work, multiple quality control measures were added to the IMT protocol, to attempt to reduce variability between animals and treatment. Originally, the bilateral injection of cancer cells were performed alone, which may have inadvertently led to an operator bias during injections. To counteract this, a second operator trained in the surgery would set-up the assembly used for injections and assist the first operator with the injections. Although the injections are performed automatically with a micro-infusion pump and therefore the opportunity to influence injections is limited, the addition of a second operator further minimizes this risk. To further reduce bias from injections, the tumor receiving IMT was not decided until the day stimulation was initiated.

Additional steps were taken to increase reliability of the hardware used to deliver stimulation. After animals were plugged into the waveform generators for stimulation,

there was a notable problem where the wires connecting the commutator to the waveform generator would be chewed through. This was because, the connection was mediated by two pins taped together, that were unstable and chewable. In collaboration with Dr. Michael Jensen and Dr. Eugene Wong in the physics department, a plastic latch was attached to the ends of the commutator that could keep the connection between the commutator and waveform generator stable. The latch was eventually used for all of our commutators, because of its increased reliability. Before surgery the cannula electrode constructs implanted were first attached to the entire stimulation apparatus, and measured with an oscilloscope. This ensured that the implanted constructs were functional and able to deliver current before surgery.

When initiating IMT a commutator plugs directly into the implanted cannula in the animal's head. The commutator has two polarized pins that must be plugged in with the correct orientation to properly deliver stimulation. Each pin must be measured with an oscilloscope to determine which orientation the commutator should be plugged in to connect with the central stimulating electrode. As well, during the 7 days of stimulation, the waveform generator output was directly measured with an oscilloscope to confirm stimulation was still being delivered into the apparatus. Unfortunately, due to the internal nature of IMT stimulation, it is not possible to directly measure the output of the central stimulating electrode while it is implanted in the brain. However, once the animal finished stimulation, the cannula electrode constructs were removed from their scalp and plugged back into the apparatus. This ensured that the electrode was not damaged during surgical implantation and stimulation, and current was still delivered through the electrode for the 7 days.

Despite the implementation of these quality control measures, it appears as if the effect of IMT has become less dramatic over the course of experiments. It is likely that the results obtained after the measures were implemented are a more reasonable approximation of IMT's effect, due to the reduced variability and increased rigor involving tumor implantation. Variability of treatment effect may exist between animals due to differences in the microenvironment surrounding the electrode, such as a blood vessel or substantial edema. This may affect the strength and spatial dimensions of the treatment and lead to differences in tumor response to treatment. It is unclear why treatment effect was more moderate after implementation of quality control measures, though it is possible that treatment effect was originally overrepresented due to inadvertent biases that were controlled for with optimization.

4.5 Cleaved caspase-3 expression in IMT treated tumors compared to sham controls

In this study, we found higher cleaved caspase-3 immuno-labelling within treated tumors compared to their sham controls. Once cleaved, caspase-3 acts as an executioner protein that irreversibly commits a cell towards apoptosis, and thus is used as a hallmark of apoptosis(Elmore, 2007; Janicke, Sprengart, Wati, & Porter, 1998; Porter & Janicke, 1999). The presence of cleaved caspase-3 in treated tumors indicates that IMT may trigger glioma cells to undergo apoptosis, leading to a decrease in tumor proliferation. This correlates with previous *in vitro* IMT results showing an increase in cleaved caspase-3 immuno-labelling after 72 hours of treatment(Xu et al., 2016). However, the exact mechanism by which IMT induces apoptosis is still unclear.

Although the precise mechanism of AEFs are unknown as well, they have been shown to significantly increase apoptosis after 48 hours of stimulation. Interestingly, pan-caspase inhibition in combination with AEFs returned the level of apoptosis to control levels(Giladi et al., 2015). This suggests that the cell death caused by AEFs is mediated by caspase activation. Ultimately, this appears to be caused by destabilization of tubulin subunits within microtubule structures, leading to aberrant cell division and aberrant chromosome segregation(Davies, Weinberg, & Palti, 2013; Giladi et al., 2015; Pless & Weinberg, 2011; Turner, Gergel, Wu, Lacroix, & Toms, 2014).

Paclitaxel, an anti-cancer drug that prevents microtubule disassembly, causes cell death by disrupting microtubule activity, leading to aneuploidy and aberrant chromosomal segregation(Giladi et al., 2015; Lanni, Lowe, Licitra, Liu, & Jacks, 1997; von Eckardstein et al., 2005)**.** This supports the idea that microtubule disruption can cause cell death by inducing mitotic dysfunction. However, further investigation is required to better understand IMT's effect on intracellular structures, and the precise mechanisms by which it induces cell death.

We also found elevated levels of cleaved caspase-3 within the core of treated tumors and their sham controls. Gliomas proliferate rapidly, and often cannot maintain adequate vascularization throughout the entire tumor to provide oxygen and nutrients. This ultimately leads to a hypoxic tumor core, causing necrosis and apoptosis at the center of the tumor(Martínez-González, 2012). High levels of apoptosis may be found at the center of both treated and untreated tumors, and therefore using an apoptotic marker may not be the most effective method to evaluate cell death caused by treatment.

4.6 Multi-modal non-invasive imaging to track progression of F98 gliomas in Fischer rats

In this study, we established MR and BL imaging for our F98 rat glioma model, which will be used in the future to non-invasively track the therapeutic efficacy of IMT over time. Both MRI and BLI are well-established in the F98 model, and are excellent techniques to non-invasively evaluate tumor progression(Towner et al., 2013). When measuring the efficacy of a novel treatment like IMT, it is essential to quantify the effect of treatment throughout tumor progression.

In humans, MRI is an important diagnostic tool to provide information to clinicians on tumor volume and location. In a preclinical rodent model, MRI permits 3D tumor volume measurements, and includes the necrotic core to include in overall volume calculations(Blanchard et al., 2006). In BLI, tumor cells are tagged with a luciferase reporter gene before implantation, to allow for visualization of only metabolically active tumor cells. This generates an image of only tumor cells, without including edema or other inflammatory regions that may be seen on MRI. As well, the process itself is much more cost-efficient compared to an MRI. The amount of radiance emitted from the tumor can be readily measured and quantified, which permits measurement of tumor size and progression at different time points. However, the image generated is 2D and thus cannot be readily be used to calculate tumor volume(Bryant et al., 2008; Hashizume et al., 2010).

Here we have correlated tumor histology with MRI and BLI, after unilateral implantation of 40,000 F98 cells. In both imaging modalities we found a corresponding increase in tumor size, and metabolic activity over the experimental time point. Comparing the

histology to the imaging gave us a baseline level of expected tumor growth in an untreated rat. These quantifiable images will ultimately be compared to rats treated with IMT, to provide an objective measurement of the treatment effect. Using both MRI and BLI will allow for the measurement of change in both tumor morphology and structure, as well as metabolic activity. This may prove useful to thoroughly evaluate the efficacy of IMT, by providing a more well-rounded approach to assessing treatment effect(Kirschner et al., 2015).

4.7 Study Limitations

One limitation in this study is the lack of understanding of the mechanism by which IMT works. Further investigation is required to better understand the underlying cause leading to *in vitro* GBM cell death, and *in vivo* attenuation of tumor growth. Depending on the mechanism, stimulation parameters and the delivery of the treatment can be altered to best enhance treatment efficacy. Better understanding the mechanism of action may also reveal currently undetectable side effects, or synergistic drugs that can amplify IMT's tumor killing effect.

As well, a limitation in our study is that the area of electric field generated by our IMT set-up has not been determined. Although calculating the precise electric field dimensions of IMT may be difficult, mathematical simulations have been successfully used to assess the electric field range of AEFs(Lok, Hua, & Wong, 2015). Understanding the effective electric field range of IMT is critical, because IMT must encompass the entire tumor to increase the likelihood of a response to treatment. Other forms of electrotherapy tested intracranially have had poor effect when the entire tumor was not in the range of treatment(Agerholm-Larsen et al., 2011). This may account for variability in treatment

found in IMT, because tumors may occasionally be out of the range of treatment and then grow uncontrollably.

Another limitation is the current construct apparatus used to deliver IMT intratumorally. Currently the cannula and electrode are combined into one construct, to permit stimulation directly in the tumor epicentre following F98 cell implantation. However, the apparatus can be simplified to reduce confounding factors, by eliminating the need for a cannula. Instead, a Hamilton syringe could stereotactically inject cells into the coordinate, followed by implantation of an electrode construct. The construct would be similar to the one currently used, but without a cannula attached. This would eliminate the large tissue defect caused by the cannula. Further, the cannulas are made of stainless steel, which has been shown to attenuate electric field strength (Prato et al., 2013). It is possible that the cannula's presence lessens the electric field delivered to the tumor and weakens the effect of IMT. Therefore, simplifying the implanted device may dramatically increase treatment effect.

Finally, another potential limitation in our study is the quantification of tumor volume measurements using stereology. This is because the calculated volume does not take into account or distinguish between necrosis and the lesion created by the cannula electrode construct. Since the volume of the tumors is not solid all the way through, stereological analysis may overestimate the overall tumor volume. Tumor surface area may therefore be a more accurate measure to evaluate tumor size. However, when comparing IMT treated tumors to internal controls, there did not appear to be a notable difference between reductions in surface area and volume.

4.8 Future Directions

In our study we demonstrated that IMT attenuates tumor growth in a rat glioma model, and established tumor imaging modalities in our model to non-invasively track tumor progression. A critical next step in developing an animal model of IMT is to mathematically model the electric field generated by the stimulation. As previously mentioned, the precise spatial dimensions of IMT's electric field have not been investigated. If the current set-up generates a small and focal electric field, then the entire tumor may not receive the treatment effect. It is essential to further investigate the electric field size with different stimulating and reference electrode configurations to ensure the entire tumor margins are encompassed by the treatment. The electric field intensity and spatial dimensions may change depending on the location and number of stimulating and reference electrodes(Agoramurthy, Campana, & Sundararajan, 2011). Ultimately, modelling the electric field generated by IMT will permit further optimizing of the electrode configuration. This may lead to greater efficacy and reproducibility of IMT *in vivo*.

Currently, the standard of care for treating GBM is surgical resection of the tumor followed by adjuvant chemotherapy and radiation. IMT may serve as a new modality of treatment to be offered alongside existing therapies. Our lab has already shown IMT markedly enhances the effect of the chemotherapeutic TMZ *in vitro*(Xu et al., 2016). The F98 glioma model in Fischer rats has been proven to be resistant to conventional forms of therapy, much like human GBM(Hayat, 2011). Combining IMT with already existing therapies may potentiate overall treatment efficacy, without worsening side effects and patient quality of life. Future studies will investigate the clinically relevant combination

of IMT, TMZ, and radiation in the F98 glioma model to evaluate any potential synergistic or additive effects between IMT and existing therapies. As well, any potential negative side effects or interactions between treatments will be investigated.

Another potential study is a longitudinal experiment assessing the effect of IMT over an undefined period of time. Instead of bilateral tumor implantation, there would only one tumor implanted per animal. A cohort of animals would receive IMT, while another cohort would receive no treatment. Therefore, an internal control tumor is unnecessary, because the two groups would be compared to each other rather than two tumors in a single animal. Further, adding an internal untreated control tumor would shorten the lifespan of animals in both groups, and confound the potential lifespan enhancing effects of IMT. Unlike our current experimental paradigm, animals would not be sacrificed until they reached a predetermined health threshold. Ideally, the study would demonstrate a decrease in tumor growth due to IMT, correlated with a corresponding increase in lifespan. Additionally, this study could include the conventional therapies previously mentioned to assess the effect that combined therapy has on overall animal lifespan. These studies would be complemented by monitoring tumor progression with both BLI and MRI to quantify the change in tumor size over the experimental timespan. Demonstrating a quantifiable and measurable increase in lifespan with IMT would be a promising step towards the use of this treatment in the clinic.

PART 5: SUMMARY AND CONCLUSIONS

Summary and conclusions

5.1 Summary

- 40,000 F98 cells implanted into the caudate putamen had reproducible growth kinetics at the 4, 7 and 11 day post-surgery date, with robust tumors 4 days post-surgery

- IMT delivered directly to normal brain parenchyma did not cause tissue damage, necrosis, or bleeding

- Tumors treated with IMT for 7 continuous days had altered morphology and were smaller in size than their internal sham controls

- IMT treated tumors had significantly decreased surface area and volume when normalized to their sham control.

- BLI and MRI non-invasively offers the capability to measure the progression of F98 tumors in Fischer rats over the experimental time point.

5.2 Conclusion

This study established a proof of principle model of IMT in the Fischer rat glioblastoma model, and investigating the safety and efficacy of the treatment. Our findings indicate that 7 days of continuous IMT stimulation does not cause damage to normal brain parenchyma. However, we showed that 7 days of continuous IMT stimulation delivered to intracerebral gliomas attenuates tumor growth. Histological analysis of brain tissue indicated that treated tumors were smaller in size compared to their internal sham controls. As well, stereological analysis of treated tumors revealed a significant decrease in tumor surface area and volume, when normalized to their internal sham controls. Further, we successfully monitored tumor progression in our model using the non-invasive imaging modalities BLI and MRI.

This study builds on the comprehensive *in vitro* experiments previously performed that established the anti-cancer properties of IMT. With emerging evidence supporting the use of electrotherapy for GBM, it is crucial that this animal model of IMT continues to be optimized and developed. These results will guide further studies to enhance the efficacy and reproducibility of IMT, and will serve as a crucial step before clinical translation.

References

Agerholm-Larsen, B., Iversen, H. K., Ibsen, P., Moller, J. M., Mahmood, F., Jensen, K. S., & Gehl, J. (2011). Preclinical validation of electrochemotherapy as an effective treatment for brain tumors. *Cancer Research*, *71*(11), 3753–3762. http://doi.org/10.1158/0008-5472.CAN-11-0451

Agnihotri, S., Burrell, K. E., Wolf, A., Jalali, S., Hawkins, C., Rutka, J. T., & Zadeh, G. (2013). Glioblastoma, a Brief Review of History, Molecular Genetics, Animal Models and Novel Therapeutic Strategies. *Archivum Immunologiae et Therapiae Experimentalis*, *61*(1), 25–41. http://doi.org/10.1007/s00005-012-0203-0

Agoramurthy, P., Campana, L., & Sundararajan, R. (2011). Tumor Electric Field Distribution Studies using Various Electrode Configurations, 1–8.

Barker, M., Hoshino, T., Gurcay, O., & Eliason, J. (1973). Development of an Animal Brain Tumor Model and Its Response to Therapy with 1 , 3-Bis (2-chloroethyl) -1-nitrosourea Development of an Animal Brain Tumor Model and Its Response to Therapy with IjS-Bisil-chloroethylVl-nitrosourea1, *33*(May), 976–986.

Barth, R. F., & Kaur, B. (2010). Rat brain tumor models in experimental neuro-oncology: the C6,9L,T9,RG2,F98,BT4C,RT-2 and CNS-1 gliomas. *Journal of Neurooncology*, *23*(7), 1365–1371. http://doi.org/10.1016/j.tiv.2009.08.005.Copper

Berens, M. E., & Giese, a. (1999). "...those left behind." Biology and oncology of invasive glioma cells. *Neoplasia (New York, N.Y.)*, *1*(3), 208–19. http://doi.org/10.1038/sj.neo.7900034

Blanchard, J., Mathieu, D., Patenaude, Y., & Fortin, D. (2006). MR-pathological comparison in F98-Fischer glioma model using a human gantry. *The Canadian Journal of Neurological Sciences. Le Journal Canadien Des Sciences Neurologiques*, *33*(1), 86–91. Retrieved from http://www.ncbi.nlm.nih.gov/pubmed/16583728

Bondy, M. L., Scheurer, M. E., Malmer, B., Barnholtz-Sloan, J. S., Davis, F. G., Il'yasova, D., … Buffler, P. a. (2008). Brain tumor epidemiology: Consensus from the Brain Tumor Epidemiology Consortium. *Cancer*, *113*(7), 1953–1968. http://doi.org/10.1002/cncr.23741

Bryant, M. J., Chuah, T. L., Luff, J., Lavin, M. F., & Walker, D. G. (2008). A novel rat model for glioblastoma multiforme using a bioluminescent F98 cell line. *Journal of Clinical Neuroscience : Official Journal of the Neurosurgical Society of Australasia*, *15*(5), 545–51. http://doi.org/10.1016/j.jocn.2007.04.022

Canadian Cancer Society's Advisory Committee on Cancer Statistics. (2015). *Canadian Cancer Statistics 2015*. Toronto.

Davies, A. M., Weinberg, U., & Palti, Y. (2013). Tumor treating fields: a new frontier in cancer therapy. *Annals of the New York Academy of Sciences*, *1291*, 86–95. http://doi.org/10.1111/nyas.12112

Deniau, J. M., Degos, B., Bosch, C., & Maurice, N. (2010). Deep brain stimulation mechanisms: Beyond the concept of local functional inhibition. *European Journal of Neuroscience*, *32*(7), 1080–1091. http://doi.org/10.1111/j.1460-9568.2010.07413.x

Denlinger RH, Axler DA, Koestner A, L. L. (1975). Tumor-specific transplantation immunity to intracerebral challenge with cells from a methylnitrosourea-induced brain tumor. *Journal of Medicine*, *6*(3-4), 249–259.

Doblas, S., Saunders, D., Kshirsagar, P., Pye, Q., Oblander, J., Gordon, B., … Towner, R. a. (2008). Phenyl-tert-butylnitrone induces tumor regression and decreases angiogenesis in a C6 rat glioma model. *Free Radical Biology and Medicine*, *44*(1), 63–72. http://doi.org/10.1016/j.freeradbiomed.2007.09.006

Elmore, S. (2007). Apoptosis: a review of programmed cell death. *Toxicologic Pathology*, *35*(4), 495–516. http://doi.org/10.1080/01926230701320337

Furnari, F. B., Fenton, T., Bachoo, R. M., Mukasa, A., Stommel, J. M., Stegh, A., … Cavenee, W. K. (2007). Malignant astrocytic glioma : genetics , biology , and paths to treatment, 2683–2710. http://doi.org/10.1101/gad.1596707.instability.

Garcion, E., Lamprecht, A., Heurtault, B., Paillard, A., Aubert-Pouessel, A., Denizot, B., … Benoît, J.-P. (2006). A new generation of anticancer, drug-loaded, colloidal vectors reverses multidrug resistance in glioma and reduces tumor progression in rats. *Molecular Cancer Therapeutics*, *5*(7), 1710–1722. http://doi.org/10.1158/1535-7163.MCT-06-0289

Gehl, J. (2003). Electroporation: theory and methods, perspectivesfor drug delivery, gene therapy and research. *Acta Physiol Scand*, *177*, 437–447.

Gehl, J., Sørensen, T. H., Nielsen, K., Raskmark, P., Nielsen, S. L., Skovsgaard, T., & Mir, L. M. (1999). In vivo electroporation of skeletal muscle: Threshold, efficacy and relation to electric field distribution. *Biochimica et Biophysica Acta - General Subjects*, *1428*(2-3), 233–240. http://doi.org/10.1016/S0304-4165(99)00094-X

Giladi, M., Schneiderman, R. S., Voloshin, T., Porat, Y., Munster, M., Blat, R., … Palti, Y. (2015). Mitotic Spindle Disruption by Alternating Electric Fields Leads to Improper Chromosome Segregation and Mitotic Catastrophe in Cancer Cells. *Scientific Reports*, *5*(November), 18046. http://doi.org/10.1038/srep18046

Grobben, B., De Deyn, P. P., & Slegers, H. (2002). Rat C6 glioma as experimental model system for the study of glioblastoma growth and invasion. *Cell and Tissue Research*, *310*(3), 257–270. http://doi.org/10.1007/s00441-002-0651-7

Guo, F., Ph, D., Yao, C., Ph, D., Li, C., Ph, D., … Ph, D. (2014). In Vivo Evidences of Nanosecond Pulsed Electric Fields for Melanoma Malignancy Treatment on Tumor-bearing BALB / c Nude Mice, *13*(4). http://doi.org/10.7785/tcrt.2012.500385

Guo, P., Hu, B., Gu, W., Xu, L., Wang, D., Huang, H.-J. S., … Cheng, S.-Y. (2003). Platelet-derived Growth Factor-B Enhances Glioma Angiogenesis by Stimulating Vascular Endothelial Growth Factor Expression in Tumor Endothelia and by

Promoting Pericyte Recruitment. *The American Journal of Pathology*, *162*(4), 1083–1093. http://doi.org/10.1016/S0002-9440(10)63905-3

Hashizume, R., Ozawa, T., Dinca, E. B., Banerjee, A., Prados, M. D., James, C. D., & Gupta, N. (2010). A human brainstem glioma xenograft model enabled for bioluminescence imaging. *Journal of Neuro-Oncology*, *96*(2), 151–159. http://doi.org/10.1007/s11060-009-9954-9

Hayat, M. a. (2011). *Tumors of the Central Nervous System, Volume 2*. http://doi.org/10.1007/978-94-007-0618-7

Heimberger, A. B., Suki, D., Yang, D., Shi, W., & Aldape, K. (2005). The natural history of EGFR and EGFRvIII in glioblastoma patients. *Journal of Translational Medicine*, *3*, 38. http://doi.org/10.1186/1479-5876-3-38

Holland, E. C. (2000). Glioblastoma multiforme: the terminator. *Proceedings of the National Academy of Sciences of the United States of America*, *97*(12), 6242–6244.

Horikoshi, T., Naganuma, H., Ohashi, Y., Ueno, T., & Nukui, H. (2000). Enhancing effect of electric stimulation on cytotoxicity of anticancer agents against rat and human glioma cells, *51*(5), 371–378.

James L. Fisher, Judith A. Schwartzbaum, Margaret Wrensch, J. L. W. (2007). Epidemiology of brain tumours. *Neurologic Clinics*, *25*(4), 867–890. http://doi.org/doi:10.1016/j.ncl.2007.07.002

Janicke, R. U., Sprengart, M. L., Wati, M. R., & Porter, a G. (1998). Caspase-3 is required for DNA fragmentation and morphological changes associated with apoptosis. *J. Biol. Chem.*, *273*(16), 9357–9360. http://doi.org/10.1074/jbc.273.16.9357

Johnson, M. D., & McIntyre, C. C. (2008). Quantifying the neural elements activated and inhibited by globus pallidus deep brain stimulation. *Journal of Neurophysiology*, *100*(5), 2549–2563. http://doi.org/10.1152/jn.90372.2008

Kaur, R. F. B. and B. (2010). Rat Brain tumor models in experimental neuro-oncology: the C6, 9L, T9, RG2, F98, BT4C, RT-2, and CNS-1 gliomas. *Neuro-Oncology*, *94*(3), 299–312. http://doi.org/10.1007/s11060-009-9875-7.Rat

Kirschner, S., Felix, M. C., Hartmann, L., Bierbaum, M., Maros, M. E., Kerl, H. U., … Brockmann, M. a. (2015). In vivo micro-CT imaging of untreated and irradiated orthotopic glioblastoma xenografts in mice: capabilities, limitations and a comparison with bioluminescence imaging. *Journal of Neuro-Oncology*, *122*(2), 245–254. http://doi.org/10.1007/s11060-014-1708-7

Kirson, E. D., Dbalý, V., Tovarys, F., Vymazal, J., Soustiel, J. F., Itzhaki, A., … Palti, Y. (2007). Alternating electric fields arrest cell proliferation in animal tumor models and human brain tumors. *Proceedings of the National Academy of Sciences of the United States of America*, *104*(24), 10152–7. http://doi.org/10.1073/pnas.0702916104

Kirson, E. D., Gurvich, Z., Schneiderman, R., Dekel, E., Itzhaki, A., Wasserman, Y., … Palti, Y. (2004). Disruption of Cancer Cell Replication by Alternating Electric Fields Disruption of Cancer Cell Replication by Alternating Electric Fields, 3288–3295.

Kobayashi, N., Allen, N., Clendenon, N. R., & Ko, L. W. (1980). An improved rat brain-tumor model. *Journal of Neurosurgery*, *53*(6), 808–815. http://doi.org/10.3171/jns.1980.53.6.0808

Lampson, L. a. (2001). New animal models to probe brain tumor biology, therapy, and immunotherapy: Advantages and remaining concerns. *Journal of Neuro-Oncology*, *53*(3), 275–287. http://doi.org/10.1023/A:1012230113527

Lanni, J. S., Lowe, S. W., Licitra, E. J., Liu, J. O., & Jacks, T. (1997). P53-Independent Apoptosis Induced By Paclitaxel Through an Indirect Mechanism. *Proc Natl Acad Sci U S A*, *94*(18), 9679–9683. http://doi.org/10.1073/pnas.94.18.9679

Li, K., Han, H., Zhu, K., Lee, K., Liu, B., Zhou, F., … He, Q. (2013). Real-time magnetic resonance imaging visualization and quantitative assessment of diffusion in the cerebral extracellular space of C6 glioma-bearing rats. *Neuroscience Letters*, *543*, 84–89. http://doi.org/10.1016/j.neulet.2013.02.071

Lok, E., Hua, V., & Wong, E. T. (2015). Computed modeling of alternating electric fields therapy for recurrent glioblastoma. *Cancer Medicine*, 1697–1699. http://doi.org/10.1002/cam4.519

Louis, D. N., Ohgaki, H., Wiestler, O. D., Cavenee, W. K., Burger, P. C., Jouvet, A., … Kleihues, P. (2007). The 2007 WHO classification of tumours of the central nervous system. *Acta Neuropathologica*, *114*(2), 97–109. http://doi.org/10.1007/s00401-007-0243-4

Mahmood, F., & Gehl, J. (2011). Optimizing clinical performance and geometrical robustness of a new electrode device for intracranial tumor electroporation. *Bioelectrochemistry*, *81*(1), 10–16. http://doi.org/10.1016/j.bioelechem.2010.12.002

Markx, G. H. (2008). The use of electric fields in tissue engineering. *Organogenesis*, *4*(1), 11–17. http://doi.org/10.4161/org.5799

Martínez-González, A., Calvo, G. F., Pérez Romasanta, L. a., & Pérez-García, V. M. (2012). Hypoxic Cell Waves Around Necrotic Cores in Glioblastoma: A Biomathematical Model and Its Therapeutic Implications. *Bulletin of Mathematical Biology*, *74*(12), 2875–2896. http://doi.org/10.1007/s11538-012-9786-1

Mathieu, D., Lamarche, J. B., & Fortin, D. (2005). The Importance of a Syngeneic Glioma Implantation Model : Comparison of the F98 Cell Line in Fischer and Long-Evans Rats. *Journal Of Applied Research*, *5*(1), 17–25.

Mathieu, D., Lecomte, R., Tsanaclis, A. M., Larouche, A., & Fortin, D. (2007). Standardization and detailed characterization of the syngeneic Fischer/F98 glioma model. *The Canadian Journal of Neurological Sciences. Le Journal Canadien Des Sciences Neurologiques*, *34*(3), 296–306.

McCaig, C. D., Rajnicek, A. M., Song, B., & Zhao, M. (2005). Controlling cell behavior electrically: current views and future potential. *Physiological Reviews*, *85*(3), 943–978. http://doi.org/10.1152/physrev.00020.2004.

Mcgarrity, G. J., & Chiang, Y. A. W. E. N. L. (1995). Effect o f H e r p e s S i m p l e x V i r u s T h y m i d i n e K i n a s e Levels o n Ganciclovir-Mediated Expression the Cytotoxicity a n d " Bystander Effect " CHEAU-YUN CHEN , YUNG-NIEN CHANG , PATRICIA RYAN , MICHELLE LINSCOTT , UK)., *1476*(November), 1467–1476.

McIntosh, J., Grishchuk, E., & West, R. (2002). Chromosome-microtubule interactions during mitosis. *Annu Review Cell Developmental Biology*, *18*, 193–219.

Miklavcic, D., Beravs, K., Semrov, D., Cemazar, M., Demsar, F., & Sersa, G. (1998). The importance of electric field distribution for effective in vivo electroporation of tissues. *Biophysical Journal*, *74*(5), 2152–2158. http://doi.org/10.1016/S0006-3495(98)77924-X

Miklavcic, D., Snoj, M., Zupanic, A., Kos, B., Cemazar, M., Kropivnik, M., … Sersa, G. (2010). Towards treatment planning and treatment of deep-seated solid tumors by electrochemotherapy. *Biomedical Engineering Online*, *9*, 10. http://doi.org/10.1186/1475-925X-9-10

Miyake, J. A., Benadiba, M., Ribeiro, G., De Oliveira Silva, D., & Colquhoun, A. (2014). Novel Ruthenium - Gamma-linolenic acid complex inhibits C6 rat glioma cell proliferation In Vitro and in the orthotopic C6 model In Vivo after osmotic pump infusion. *Anticancer Research*, *34*(4), 1901–1912.

Morantz, R. a, Wood, G. W., Foster, M., Clark, M., & Gollahon, K. (1979). Macrophages in experimental and human brain tumors. Part 2: studies of the macrophage content of human brain tumors. *Journal of Neurosurgery*, *50*(3), 305–311. http://doi.org/10.3171/jns.1979.50.3.0298

Mrugala, M. M., Engelhard, H. H., Dinh Tran, D., Kew, Y., Cavaliere, R., Villano, J. L., … Butowski, N. (2014). Clinical practice experience with NovoTTF-100A??? system for glioblastoma: The patient registry dataset (PRiDe). *Seminars in Oncology*, *41*(S6), S4–S13. http://doi.org/10.1053/j.seminoncol.2014.09.010

Nabors, L. B., Portnow, J., Ammirati, M., Brem, H., Brown, P., Butowski, N., … Ho, M. (2014). Central nervous system cancers, version 2.2014. Featured updates to the NCCN Guidelines. *Journal of the National Comprehensive Cancer Network : JNCCN*, *12*(11), 1517–23. http://doi.org/10.1007/s00330-006-0435-7

Neal, R. E., Rossmeisl, J. H., D'Alfonso, V., Robertson, J. L., Garcia, P. a., Elankumaran, S., & Davalos, R. V. (2014). In vitro and numerical support for combinatorial irreversible electroporation and electrochemotherapy glioma treatment. *Annals of Biomedical Engineering*, *42*(3), 475–487. http://doi.org/10.1007/s10439-013-0923-2

Ohgaki, H., Dessen, P., Jourde, B., Horstmann, S., Nishikawa, T., Di Patre, P. L., … Kleihues, P. (2004). Genetic pathways to glioblastoma: a population-based study. *Cancer Research*, *64*(19), 6892–6899. http://doi.org/10.1158/0008-5472.can-04-1337

Orlowski, S., Belehradek, J., Paoletti, C., & Mir, L. (1988). Transient electropermeabilization of cells in culture: Increase of the cytotoxicity of anticancer drugs. *Biochemical Pharmacology*, *37*(24), 4727–4733.

Ostrom, Q. T., Gittleman, H., Farah, P., Ondracek, A., Chen, Y., Wolinsky, Y., … Barnholtz-sloan, J. S. (2013). N E U RO - O N CO LO GY CBTRUS Statistical Report : Primary Brain and Central Nervous System Tumors Diagnosed in the United States in 2006-2010.

Parsa, A.T., et al. (2000). Limitations of the C6/Wistar Intracerebral Glioma Model: Implications for immunotherapy. *Neurosurgery*, *47*(4), 993–1000.

Pereira, E. a C., Green, A. L., Nandi, D., & Aziz, T. Z. (2007). Deep brain stimulation: indications and evidence. *Expert Review of Medical Devices*, *4*(5), 591–603. http://doi.org/10.1586/17434440.4.5.591

Peterson, D. L., Snerioan, P. J., Ph, D., & Brown, W. E. (1994). Animal models for brain tumors historical perspectives.pdf, 865–876.

Pless, M., & Weinberg, U. (2011). Tumor treating fields: concept, evidence and future. *Expert Opinion on Investigational Drugs*, *20*(8), 1099–106. http://doi.org/10.1517/13543784.2011.583236

Porter, a G., & Janicke, R. U. (1999). Emerging roles of caspase-3 in apoptosis. *Cell Death and Differentiation*, *6*(2), 99–104. http://doi.org/10.1038/sj.cdd.4400476

Prato, F. S., Desjardins-Holmes, D., Keenliside, L. D., DeMoor, J. M., Robertson, J. a, & Thomas, a W. (2013). Magnetoreception in laboratory mice: sensitivity to extremely low-frequency fields exceeds 33 nT at 30 Hz. *J R Soc Interface*, *10*(81), 20121046. http://doi.org/10.1098/rsif.2012.1046

Pudenz, R. (1976). Adverse effects of electrical energy applied to the nervous system. *Neurosurgery*, *1*(2), 190–191.

Rehman, A., Elmore, K., & Mattei, T. (2015). The effects of alternating electric fields in glioblastoma: current evidence on therapeutic mechanisms and clinical outcomes. *Neurosurgical Focus*, *38*(3), 1–10.

Reilly, K. M., Rubin, J. B., Gilbertson, R. J., Garbow, J. R., Roussel, M. F., & Gutmann, D. H. (2008). Rethinking brain tumors: The fourth Mouse Models of Human Cancers Consortium nervous system tumors workshop. *Cancer Research*, *68*(14), 5508–5511. http://doi.org/10.1158/0008-5472.CAN-08-0703

Repacholi, M. H., & Greenebaum, B. (1999). Interaction of static and extremely low frequency electric and magnetic fields with living systems: health effects and research needs. *Bioelectromagnetics*, *20*(3), 133–160. http://doi.org/10.1002/(sici)1521-186x(1999)20:3<133::aid-bem1>3.0.co;2-o

Results, P. P. (1986). : Acta- Ncurochirurgica Current Brain Tumour Models with Particular Consideration Outline of Literature and Personal Preliminary Results, *41*, 35–41.

Saini, M., Roser, F., Samii, M., & Bellinzona, M. (2004). A model for intratumoural chemotherapy in the rat brain. *Acta Neurochirurgica*, *146*(7), 731–734. http://doi.org/10.1007/s00701-004-0261-0

Schepkin, V. D., Lee, K. C., Kuszpit, K., Muthuswami, M., Timothy, D., Chenevert, T. L., … Ross, B. D. (2011). Proton and sodium MRI assessment of emerging tumor chemotherapeutic resistance. *NMR Biomed*, *19*(8), 1035–1042. http://doi.org/10.1002/nbm.1074.Proton

Sersa, G., Teissie, J., Cemazar, M., Signori, E., Kamensek, U., Marshall, G., & Miklavcic, D. (2015). Electrochemotherapy of tumors as in situ vaccination boosted by immunogene electrotransfer. *Cancer Immunology, Immunotherapy*. http://doi.org/10.1007/s00262-015-1724-2

Sibenaller, Z. a, Etame, A. B., Ali, M. M., Barua, M., Braun, T. a, Casavant, T. L., & Ryken, T. C. (2005). Genetic characterization of commonly used glioma cell lines in the rat animal model system. *Neurosurgical Focus*, *19*(4), E1. http://doi.org/10.3171/foc.2005.19.4.2

Stupp, R., & et al. (2015). Maintenance therapy with tumor-treating fields plus temozolomide vs temozolomide alone for glioblastoma. *JAMA*, *314*(23).

Stupp, R., Mason, W. P., van den Bent, M. J., Weller, M., Fisher, B., Taphoorn, M. J. B., … Mirimanoff, R. O. (2005). Radiotherapy plus concomitant and adjuvant temozolomide for glioblastoma. *The New England Journal of Medicine*, *352*(10), 987–96. http://doi.org/10.1056/NEJMoa043330

Stupp, R., Wong, E. T., Kanner, A. a, Steinberg, D., Engelhard, H., Heidecke, V., … Gutin, P. H. (2012). NovoTTF-100A versus physician's choice chemotherapy in recurrent glioblastoma: a randomised phase III trial of a novel treatment modality.

European Journal of Cancer (Oxford, England : 1990), *48*(14), 2192–202. http://doi.org/10.1016/j.ejca.2012.04.011

Tang, L., Yao, C., & Sun, C. (2009). Apoptosis induction with electric pulses - A new approach to cancer therapy with drug free. *Biochemical and Biophysical Research Communications*, *390*(4), 1098–1101. http://doi.org/10.1016/j.bbrc.2009.10.092

Tanriover, N., Ulu, M. O., Sanus, G. Z., Bilir, A., Canbeyli, R., Oz, B., … Kuday, C. (2008). The effects of systemic and intratumoral interleukin-12 treatment in C6 rat glioma model. *Neurological Research*, *30*(5), 511–7. http://doi.org/10.1179/174313208X289516

The Deep-Brain Stimulation for Parkinson's Disease Study Group, & The Deep-Brain Stimulation for Parkinson's Disease Study, G. (2001). Deep-Brain Stimulation of the Subthalamic Nucleus or the Pars Interna of the Globus Pallidus in Parkinson's Disease. *N Engl J Med*, *345*(13), 956–963. http://doi.org/10.1056/NEJMoa000827

Tonn, J.-C. (2002). Research and Publishing in Neurosurgery. In Y. Kanpolat (Ed.), (pp. 79–83). Vienna: Springer Vienna. http://doi.org/10.1007/978-3-7091-6743-4_13

Towner, R. a., Gillespie, D. L., Schwager, A., Saunders, D. G., Smith, N., Njoku, C. E., … Jensen, R. L. (2013). Regression of glioma tumor growth in F98 and U87 rat glioma models by the Nitrone OKN-007. *Neuro-Oncology*, *15*(3), 330–340. http://doi.org/10.1093/neuonc/nos337

Turner, S. G., Gergel, T., Wu, H., Lacroix, M., & Toms, S. a. (2014). The effect of field strength on glioblastoma multiforme response in patients treated with the NovoTTF^{TM}-100A system. *World Journal of Surgical Oncology*, *12*(March), 162. http://doi.org/10.1186/1477-7819-12-162

Verma, M. (2009). *Cancer Epidemiology*. *Cancer Epidemology Vol 2 Modifiable Factors*. http://doi.org/10.1007/978-1-60327-492-0

Von Eckardstein, K. L., Patt, S., Kratzel, C., Kiwit, J. C. W., & Reszka, R. (2005). Local chemotherapy of F98 rat glioblastoma with paclitaxel and carboplatin embedded in

liquid crystalline cubic phases. *Journal of Neuro-Oncology*, *72*(3), 209–215. http://doi.org/10.1007/s11060-004-3010-6

Wen, P., & Kesari, S. (2008). Malignant Gliomas in Adults — NEJM. *Malignant Gliomas in Adults*, 492–507. http://doi.org/10.1056/NEJMc086380

Xu, H. U., Bihari, F., Whitehead, S., Wong, E., Schmid, S., & Hebb, M. O. (2016). In Vitro Validation of Intratumoral Modulation Therapy for Glioblastoma, *80*, 71–80.

Zimmermann, U. (1982). Electric field-mediated fusion and related electrical phenomena. *BBA - Reviews on Biomembranes*, *694*(3), 227–277. http://doi.org/10.1016/0304-4157(82)90007-7

Curriculum Vitae

EDUCATION

Undergraduate Degree in Medical Sciences at Western University
Bachelor of Medical Sciences
Honors Specialization in Medical Science with distinction, 2014

Graduate Degree in Anatomy and Cell Biology at Western University
Master's Degree in Anatomy and Cell Biology
Neurobiological Sciences, 2016

TEACHING EXPERIENCE

Graduate Teaching Assistant – Western University
- Neuroscience 9550, September – April 2015-2016

AWARDS AND ACCOMPLISHMENTS

Dean's List at Western University, 2011-2014

Western Scholarship of Excellence, 2010-2011
One-year $2000 Scholarship

Western Graduate Research Scholarship, 2014-2016
One-year $4500 Scholarship x2

Lawson Internal Research Fund Scholarship, 2014-2015
One-year $15,000 Scholarship

CONTRIBUTIONS TO CONFERENCES

ORAL PRESENTATIONS

Cooper M, Di Sebastiano A, Xu H, de Oliveira C, Whitehead S, Schmid S, Hebb M (2015) Intratumoral modulation therapy for glioblastoma. *Clinical Neurological Sciences Research Day, London.*

SUBMITTED ABSTRACTS

Cooper M, Di Sebastiano A, Schmid S, Hebb M (2015) Intratumoral modulation therapy for glioblastoma. *Southern Ontario Neuroscience Association, London.*

Cooper M, Schmid S, Hebb M (2015) Intratumoral modulation therapy for glioblastoma. *Anatomy and Cell Biology Research Day, London.*

Cooper M, Xu H, de Oliveira C, Whitehead S, Schmid S, Hebb M (2015) Intratumoral modulation therapy for glioblastoma. *Society for Neuroscience, Chicago*.

Xu H, ***Cooper M***, de Oliveira C, Wong E, Schmid S, Hebb M (2015) Intratumoral modulation therapy for glioblastoma. *Global Biotechnology Congress, Boston.*

Cooper M, Xu H, de Oliveira C, Wong E, Schmid S, Hebb M (2015) Intratumoral modulation therapy for glioblastoma. *Oncology Research and Education Day, London*.

Cooper M, Schmid S, Hebb M (2015) Heat Shock Protein 27 as a therapeutic target in glioblastoma multiforme. *Southern Ontario Neuroscience Association, Hamilton.*

Cooper M, Schmid S, Hebb M (2015) Heat Shock Protein 27 as a therapeutic target in glioblastoma multiforme. *London Health Research Day, London.*

Cooper M, Schmid S, Hebb M (2014) Heat Shock Protein 27 as a therapeutic target in glioblastoma multiforme. *Anatomy and Cell Biology Research Day, London.*